Astronomy & Astrophysics

A spectroscopic survey of the youngest field stars in the solar neighborhood

II. The optically faint sample ⋆,⋆⋆

A. Frasca[1], P. Guillout[2], A. Klutsch[1], R. Freire Ferrero[2,†], E. Marilli[1], K. Biazzo[1], D. Gandolfi[3], and D. Montes[4]

[1] INAF - Osservatorio Astrofisico di Catania, via S. Sofia, 78, 95123 Catania, Italy
e-mail: antonio.frasca@oact.inaf.it
[2] Université de Strasbourg, CNRS, Observatoire astronomique de Strasbourg, UMR 7550, 67000 Strasbourg, France
[3] Dipartimento di Fisica, Università di Torino, via P. Giuria, 1, 10125 Torino, Italy
[4] Departamento de Astrofísica y Ciencias de la Atmósfera, Universidad Complutense de Madrid, 28040 Madrid, Spain

ABSTRACT

Context. Star formation in the solar neighborhood is mainly traced by young stars in open clusters, associations, and in the field, which can be identified, for example, by their X-ray emission. The determination of stellar parameters for the optical counterparts of X-ray sources is crucial for a full characterization of these stars.

Aims. This work extends the spectroscopic study of the *RasTyc* sample, obtained by the cross-correlation of the *Tycho* and ROSAT All-Sky Survey catalogs, to stars fainter than $V = 9.5$ mag and aims to identify sparse populations of young stars in the solar neighborhood.

Methods. We acquired 625 high-resolution spectra for 443 presumably young stars with four different instruments in the northern hemisphere. The radial and rotational velocity ($v \sin i$) of our targets were measured by means of the cross-correlation technique, which is also helpful to discover single-lined (SB1), double-lined spectroscopic binaries (SB2), and multiple systems. We used the code ROTFIT to perform an MK spectral classification and to determine the atmospheric parameters ($T_{\rm eff}$, $\log g$, [Fe/H]) and $v \sin i$ of the single stars and SB1 systems. For these objects, we used the spectral subtraction of slowly rotating templates to measure the equivalent widths of the Hα and Li I 6708 Å lines, which enabled us to derive their chromospheric activity level and lithium abundance. We made use of *Gaia* DR1 parallaxes and proper motions to locate the targets in the Hertzsprung-Russell (HR) diagram and to compute the space velocity components of the youngest objects.

Results. We find a remarkable percentage (at least 35%) of binaries and multiple systems. On the basis of the lithium abundance, the sample of single stars and SB1 systems appears to be mostly (∼60%) composed of stars younger than the members of the UMa cluster. The remaining sources are in the age range between the UMa and Hyades clusters (∼20%) or older (∼20%). In total, we identify 42 very young (PMS-like) stars, which lie above or very close to the Pleiades upper envelope of the lithium abundance. A significant percentage (∼12%) of evolved stars (giants and subgiants) is also present in our sample. Some of these stars (∼36%) are also lithium rich ($A(\rm Li) > 1.4$).

Key words. stars: fundamental parameters – stars: chromospheres – stars: pre-main sequence – binaries: spectroscopic – techniques: spectroscopic – X-rays: stars

1. Introduction

It has been shown that open clusters (OCs) cannot account for the total star formation in the Galaxy, but can only account for about 50% at most; the remaining occur in OB associations (see, e.g., Piskunov et al. 2008; Zinnecker 2008). Although at the end of their parent cloud collapse newly formed stars are located in the same region of space, many events tend to carry these stars away from each other. After they are mixed with the stellar population of the Galactic plane, young stars are hardly distinguishable from older stars. Indeed, their magnitudes and colors are similar to

the latter and there is no gas left from the parent cloud that can help to identify the young stars. Other properties related to their young age, such as their kinematics, magnetic activity, infrared (IR) excess, and the presence of lithium in their atmospheres, must be used to spot these stars among the older population.

The most favorite scenario in the recent history of star formation in the solar neighborhood is that of a large structure in which giant molecular clouds generated massive stars about 50 Myr ago. The latter, exploding as supernovae, triggered star formation in a ring-like structure known as the Gould Belt (see, e.g., Comerón & Torra 1994; Bally 2008, and references therein) and cleaned the region around the Sun from the residual gas, generating the local bubble (see, e.g., Bonchkarev 1984; Gehrels & Chen 1993). Many OB associations and star forming regions (SFRs) within 500–600 pc are known to be part of the Gould Belt (Elias et al. 2009; Bobylev 2014).

Most studies on young low-mass stars in the solar vicinity were focused on SFRs or young OCs that represent homogeneous samples in terms of age and chemical composition.

⋆ Based on observations collected at the Italian Telescopio Nazionale *Galileo* (TNG) operated by the Fundación Galileo Galilei – INAF (Canary Islands, Spain), at the Observatoire de Haute Provence (OHP, France), and the Osservatorio Astrofisico di Catania (OAC, Italy)

⋆⋆ Tables A.1–A.4 are only available at the CDS via anonymous ftp to cdsarc.u-strasbg.fr (130.79.128.5) or via http://cdsarc.u-strasbg.fr/viz-bin/qcat?J/A+A/612/A96

† Rubens Freire Ferrero passed away on September 10, 2015.

However, sparse populations of late-type young stars apparently unrelated to known SFRs and young OCs have been discovered (e.g., Guillout et al. 1998a, and references therein). Various scenarios, such as ejection from their birth sites by close encounters (Sterzik et al. 1995) or by a very fast dispersion of small clouds (Feigelson 1996), have been proposed to explain these sources scattered over the sky. Depending on their sky position, these sources could also be related to star formation in the Gould Belt (e.g., Biazzo et al. 2012a, and references therein).

To pick up isolated young stars scattered over the whole sky, Guillout et al. (1999) cross-correlated the ROSAT All-Sky Survey (RASS; Voges et al. 1999) and the *Tycho* (or HIPPARCOS) catalogs (ESA 1997). This selection produced the so-called *RasTyc* and *RasHip* samples, containing about 14 000 and 6200 active stars, respectively. These samples are very suitable for the study of the large-scale distribution of X-ray active stars in the solar neighborhood and led to the discovery of the late-type stellar population of the Gould Belt (Guillout et al. 1998a,b). A similar approach was followed by Haakonsen & Rutledge (2009) who made a statistical cross-association of the ROSAT bright source catalog with the 2MASS point source catalog (Cutri et al. 2003). However, complementary optical data are absolutely needed for a full and safe exploitation of the huge scientific potential of the *RasTyc* and *RasHip* samples, and to search for young field stars unrelated to the main nearby SFRs and young associations.

To this aim we started a large program to follow up spectroscopically a large portion of the *RasTyc* sample observable from the northern hemisphere. The results of the optically bright ($V_T \leq 9.5$ mag) subsample were presented in Guillout et al. (2009, hereafter Paper I). In that paper, we analyzed high-resolution spectra of 426 stars with no previous spectroscopic data and found that this sample is mainly composed of stars with ages between 100 and 600 Myr, and there is a minor contribution from an older population (1–2 Gyr). A high percentage of binaries and lithium-rich giants ($\approx30\%$), which can be considered as contaminants, was also found. Based on their high lithium abundance, we also uncovered seven very young (*age* ≤ 30 Myr) stars, which appear to be unrelated to any know SFR. Some of these are good post-T Tau candidates and five are likely members of Pleiades or Castor stellar kinematic groups.

In the present paper we extend this study to the optically faint ($V > 9.5$ mag) *RasTyc* sources. The inclusion of optically fainter sources in the total sample of investigated *RasTyc* stars improves the statistics and allows us to reach a larger distance or intrinsically fainter objects.

A first result of the optically faint sample was the discovery of four lithium-rich stars packed within a few degrees on the sky in front of an area void of interstellar matter in the Cepheus complex. These stars, which form a homogeneous moving group, are likely 10–30 Myr in age. We published a preview of the results for these four stars in Guillout et al. (2010), but we include these four stars in the present paper where additional spectra have also been analyzed.

The paper is organized as follows. In Sect. 2 we present the data set and a brief description of the observations and spectra reduction. In Sect. 3 we describe the analysis aimed at measuring radial and rotational velocities (Sects. 3.1 and 3.2), atmospheric parameters (Sect. 3.3), chromospheric emission fluxes, and lithium equivalent widths (Sect. 3.4). The results are presented in Sect. 4, where the properties and evolutionary status of the targets are discussed on the basis of their position on the Hertzsprung-Russell (HR) diagram (Sect. 4.2), abundance of lithium and Hα emission (Sects. 4.3 and 4.6), kinematics

(Sect. 4.8), and spectral energy distribution (SED; Sect. 4.7). The main conclusions are summarized in Sect. 5. Individual notes on the youngest stars in our sample can be found in Appendix B.

2. Observations and reduction

We used the RasTyc catalog (Guillout et al. 1999) to obtain a statistically significant sample of the youngest field stars in the solar neighborhood. We adopted the criteria described in Paper I to select the optically fainter sources to be investigated spectroscopically for this study. These criteria are briefly summarized as

- declination $\Delta \geq 0°$ to observe the targets with telescopes located in the northern hemisphere;
- right ascension between 15 h and 8 h;
- $0.6 \leq (B - V)_T \leq 1.3$, which is the range in which the lithium $\lambda6707.8$ Å line can be used as an age indicator;
- ROSAT PSPC count rate greater than or equal to 0.03 cts s^{-1} to avoid RASS scanning bias (see Guillout et al. 1999); and
- $V_T \leq 10.5$ mag, since the *Tycho* catalog is largely incomplete above this limit.

As we observed many targets from La Palma, the first selection criterion has been slightly relaxed, such that this sample also contains some objects with negative declination ($\Delta \geq -15°$). This allowed us to compare our results with those of the SACY survey (Torres et al. 2006) of southern stellar X-ray sources.

We made a detailed search of previous data and works dealing with these sources in the Simbad and Vizier astronomical databases. We did not observe the stars whose physical parameters were already derived in the literature from high-resolution spectra. However, a few stars with published high-resolution spectra are present in our list either because they were purposely selected for comparison with the results of previous surveys or because their data were published after the approval of our observation proposals. Moreover, when two stars of similar brightness are located near the X-ray source within the typical ROSAT positional accuracy of 30″ (Voges et al. 1999), we decided to observe both of them.

We observed 134 optically faint stars from November 2001 to August 2005 with the spectrograph AURELIE at the 1.52 m telescope at the Observatoire de Haute Provence (OHP, France; see Paper I for details) and 178 stars with SARG, the high-resolution spectrograph at the 3.5 m TNG telescope (Canary Islands, Spain), in 2007[1]. We chose the SARG setup with the yellow grism and the slit width of 0″8, which provides a resolving power of $R = \lambda/\Delta\lambda \simeq 57\,000$ and a spectral coverage in the range 4600–7900 Å. Exposure times ranged from 4 to 35 minutes, according to the star magnitude, and allowed us to reach a signal-to-noise (S/N) ratio from 50 to 110, also depending on the seeing and sky conditions. Ten stars were observed in August 2009 and June 2011 with SARG and the red grism, which covers the wavelength range 5500–11 000 Å[2]. We adopted the same slit as for the previous spectra.

Moreover, 140 spectra of 120 *RasTyc* stars were acquired in 2000 and 2001 with the ELODIE échelle spectrograph ($R \simeq 42\,000$) at the 1.93 m OHP telescope. Sixty-four of these targets with $V \leq 9.5$ mag were included in the bright *RasTyc* survey (Paper I). The atmospheric parameters reported in that work were derived with the TGMET online analysis software

---

[1] Proposals TAC67-AOT15/07A and TAC35-AOT16/07B.
[2] Proposals TAC71-AOT20/09B and TAC34-AOT23/11A.

Table 1. Observing log for the full program (bright + faint sample).

Year	Period	Instrument	Resolution	Spectra
2000	Jul.–Sep.	ELODIE	42 000	83
2001	Aug.	ELODIE	42 000	57
2001	Oct.–Dec.	AURELIE	38 000	290
2002	Jun.–Nov.	AURELIE	38 000	396
2003	Jan.	AURELIE	38 000	207
2004	Jun.–Sep.	AURELIE	38 000	231
2005	Jul.–Aug.	AURELIE	38 000	126
2007	Sep.–Oct.	FRESCO	21 000	28
2007	Feb.–Dec.	SARG	57 000	184
2008	Mar.–Jul.	FRESCO	21 000	19
2009	Jun.–Oct.	FRESCO	21 000	35
2009	Aug.	SARG	57 000	4
2011	Jun.	SARG	57 000	6
Total				1666

(Katz et al. 1998) running at the 1.93 m OHP telescope. However, in the present paper we analyzed in a homogeneous way both the optically bright and faint ELODIE targets, which are all included in this study and listed in Tables A.1–A.4. Likewise, a few sources (about 25 in total) brighter than $V = 9.5$ mag without previous spectroscopic information or with incomplete data in Paper I were also observed with the other spectrographs and included in the present work.

Further observations of 30 sources were conducted in 2008 and 2009 at the 0.91 m telescope of the Osservatorio Astrofisico di Catania (OAC, Italy) with the FRESCO spectrograph that covers the spectral range 4250–6850 Å with a resolution $R \simeq 21\,000$. The S/N ratio of these spectra is in the range 40–80.

In the present paper we used a total of 625 spectra of 443 different sources taken with the aforementioned instruments, while more than 1660 spectra were acquired during about ten years for the full program (bright+faint samples). We present a concise log of the observations in Table 1.

We were not able to observe the full sample of faint *RasTyc* sources selected according to the above criteria and about 40 stars, i.e., ~10% of the sample, remained unobserved. Although a few other very young stars could have been found among this sample, the lack of their data is not expected to significantly bias our results.

Details on the reduction of spectra acquired at OHP can be found in Paper I.

The reduction of the SARG and FRESCO spectra was basically carried out inside the IRAF[3] package, following standard steps of overscan and bias subtraction, flat-field division, and scattered light subtraction. The extraction of the spectra from the prereduced images was performed with the ECHELLE task of IRAF, which allowed us to subtract the sky spectrum that was extracted from the two sides of the stellar spectrum.

Because of the gap between the two CCDs of SARG, which causes the lost of more than one échelle order, the reduction of the red and blue chip was performed separately. We paid particular care to the correction for the fringes at red and near-IR

wavelengths and to the merging of échelle orders, which was very important for the analysis of broad lines that are close to the edges of spectral orders, such as the hydrogen Hα line. For these tasks we developed ad hoc tools in IDL[4] environment. In particular, the fringe removal was accomplished by means of contemporaneous flat-field spectra that were rectified by low-order polynomial fits to obtain the fringing pattern. We optimized the fringe-correction procedure on spectra of hot and rapidly rotating stars.

Spectra of rapidly rotating AB stars (templates for telluric subtraction) and of radial and rotational velocity standard stars were also acquired with all spectrographs and were used for data analysis.

The telluric water vapor lines at the Hα and Na I D$_2$ wavelengths were subtracted using an interactive procedure described by Frasca et al. (2000) and adopting the well-exposed telluric templates acquired during the observing runs. The broad and shallow spectral lines of the latter were removed by high-order polynomial fits.

3. Data analysis

We made an analysis of the spectra with different purposes: i) to measure the radial velocity (RV) and the projected rotational velocity ($v \sin i$); ii) to determine the basic atmospheric parameters (T_{eff}, $\log g$, and [Fe/H]); iii) to evaluate the photospheric lithium content; and iv) to define the level of chromospheric activity.

We used various techniques and reached different goals and accuracies for single stars, double-lined spectroscopic binaries (SB2), and triple (SB3) or multiple systems.

3.1. Radial velocity

The measurement of RV for AURELIE and ELODIE spectra was already described in Paper I. It is based on the use of a numerical mask or a synthetic spectrum as RV template. For the ELODIE spectra this task is normally carried out by the online reduction pipeline just after the acquisition of the spectrum.

For the SARG and FRESCO échelle spectra, the RV was measured by means of the cross-correlation between the target spectrum and a template chosen among a list of spectra of RV standard stars (Table 2) that were observed with the same instrument and in the same seasons as our targets. All these stars are slow rotators and display a very low or negligible level of magnetic activity such that they were also used as non-active templates (Sect. 3.4). The cross-correlation functions (CCFs) were computed for all échelle orders but those with the lowest S/N ratio (usually for blue wavelengths). Very broad lines, such as Na I D$_2$ and Hα, and strong telluric features were excluded from the CCF analysis. The latter was performed with an ad hoc software developed by us in the IDL environment. The CCF peak was fitted with a Gaussian to evaluate its centroid and full width at half maximum (FWHM). The RV error for each spectral order, σ_i, was estimated by the fitting procedure accounting for the CCF noise (far from the peak). For a few spectra, we compared the results of our code with those from the IRAF task FXCOR, finding similar results and errors.

The final RV is obtained as the weighted mean (weight $w_i = 1/\sigma_i$) of the RV_i values measured in the individual orders. We adopted as RV uncertainty the standard error of the weighted

Table 2. Radial/rotational velocity standard stars.

Name	Sp. Type	RV (km s^{-1})	$v \sin i^d$ (km s^{-1})	Notes
HD 187691	F8 V	-0.0^a	2.8	$RV, v \sin i$
HD 102870	F8 V	4.3^a	4.5	RV
HD 157214	G0 V	-79.2^b	1.6	$v \sin i$
HD 32923	G4 V	20.50^a	1.5	$RV, v \sin i$
HD 117176	G5 V	$4.6^{b,*}$	1.2	$v \sin i$
HD 10700	G8 V	-17.1^b	0.9	$v \sin i$
HD 145675	K0 V	$-13.69^{c,*}$	0.8	$v \sin i$
HD 221354	K1 V	-25.20^a	0.6	$RV, v \sin i$
HD 115404	K2 V	7.60^a	3.3	RV
HD 182572	G8 IV	-100.35^a	1.9	$RV, v \sin i$
HD 12929	K2 III	-14.6^a	1.6	RV
HD 161096	K2 III	-12.5^a	2.1	RV

Notes. [*] Exoplanet hosting star. *RV* variable.
References. [a] Udry et al. (1999), [b] Nordström et al. (2004), [c] Nidever et al. (2002), [d] Glebocki & Gnacinski (2005).

mean, σ_{RV}. The RV values and errors for single stars or single-lined binaries (SB1) are reported in Table A.1. The targets observed more than once were classified as SB1 systems whenever the difference of two RV values is larger than the sum of the corresponding errors. A note about SB1 systems is added in Table A.4. We classified each target with a single RV measurement as a single star (S), although this does not exclude that the star could indeed be an SB1 system, or even an SB2 system observed close to the conjunction, when the lines of the individual components are fully blended.

This procedure was also used to measure the RV of the components of SB2 or multiple systems. We considered a secondary CCF peak as significant whenever it exceeded the 5σ level, where σ is the CCF noise calculated far from the peaks.

3.2. Projected rotational velocity

The $v \sin i$ was measured in two different ways. The first is based on the FWHM of the CCF peak through calibrations FWHM–$v \sin i$ obtained for several standard stars among those listed in Table 2. For each standard star, the calibration relationship was defined by measuring the FWHM of the CCF peak obtained by correlating the original spectrum with the same spectrum after being artificially broadened by the convolution with a rotation profile of increasing $v \sin i$ (from 0 to 150 km s^{-1}). We applied this method only to 21 échelle orders of the blue-chip SARG spectra covering the wavelength range from about 4900 to 6000 Å. We rejected the orders with very wide lines, which would make the results worse. The FWHM measured on the CCF of each échelle order of target spectra and RV standard stars was converted to $v \sin i$ using these calibrations. We took the average of the values for each order and the standard deviation as $v \sin i$ and error, respectively. The same procedure was applied to the FRESCO spectra, for which we used nine échelle orders in the range 5400–6400 Å, and to the single-order AURELIE spectra, for which synthetic templates were adopted (see Paper I). The measure of $v \sin i$ on the ELODIE spectra was also performed with this method. We adopted the relation proposed by Queloz et al. (1998) to convert the σ of the Gaussian fitted to the CCF peak into $v \sin i$. In a few cases, it was necessary to perform a new cross-correlation analysis on the original

ELODIE spectra to measure the RV and $v \sin i$ because the range of radial velocity encompassed by the CCF made on the fly during the observation was not sufficient. This was the case for a few very rapid rotators and SB2 systems.

This method was also used to measure the $v \sin i$ for the components of SB2 and SB3 systems. We performed independent Gaussian fits to the CCF peaks of the system components whenever they are well separated, while a double (or multiple) Gaussian fit was applied in cases of blended CCFs. In the latter case the accuracy of $v \sin i$ and RV determinations decreases with the increase of line blending and with the decrease in peak intensity. The RV and $v \sin i$ of the individual components of SB2 and SB3 spectroscopic systems are listed in Table A.2 and A.3, respectively.

The other method for measuring $v \sin i$, which can be applied only to single stars or SB1 systems, is based on the minimization of the residuals *observed − template*, where the *template* is one of the spectra in Table 2 rotationally broadened from 0 to 150 km s^{-1} with a step of 0.5 km s^{-1}. This is the same algorithm used by ROTFIT for the determination of the atmospheric parameters (see Sect. 3.3 for further details) by adopting a wider list of reference stars. For very rapid rotators, we explored a wider range of $v \sin i$ (from 0 to 500 km s^{-1}) with a larger sampling (5 km s^{-1}).

The values of $v \sin i$ obtained for single or SB1 stars with both methods, $v \sin i_{\text{CCF}}$ and $v \sin i_{\text{ROTFIT}}$, are quoted, along with their errors, in Table A.1. These values are clearly in very good agreement with each other, as shown in Fig. 1, where the two data sets follow a close one-to-one relationship. The average difference, calculated for values of $v \sin i \leq 100$ km s^{-1}, is only 0.38 km s^{-1}, which is not significant, accounting for measurement errors. The standard deviation of the residuals is 2.26 km s^{-1}. We note that the scatter enhances for the stars rotating faster than about 30 km s^{-1}, especially for the ELODIE data. This is probably due to the fit of the CCF peak, whose shape is far from a Gaussian for high $v \sin i$, and to the Queloz et al. (1998) calibration relation adopted for the ELODIE spectra, which has a full validity for $v \sin i$ up to 20 km s^{-1}. A few discrepant values around 10 km s^{-1} are visible for the FRESCO data. This is likely the result of the lower resolution of this instrument for which the minimum detectable $v \sin i$ is about 5–7 km s^{-1}. From the above arguments, we consider as most reliable the values derived with ROTFIT, which are used in the following.

3.3. Atmospheric parameters and spectral classification

The MK spectral classification and determination of the basic atmospheric parameters (T_{eff}, $\log g$, and [Fe/H]) were performed by means of the code ROTFIT (Frasca et al. 2006). We adopted, as templates, a library of 270 high-resolution spectra of slowly rotating stars with well-known parameters (Soubiran et al. 2010) spanning a wide range of effective temperature, gravity, and iron abundance, which were retrieved from the ELODIE Archive (Moultaka et al. 2004).

The SARG spectra ($R_{\text{SARG}} = 57\,000$) were degraded to the ELODIE resolution ($R_{\text{ELODIE}} = 42\,000$) by means of the convolution with a Gaussian kernel of width $W = \lambda \sqrt{1/R_{\text{ELODIE}}^2 - 1/R_{\text{SARG}}^2}$ Å. We applied ROTFIT only to the échelle orders with the best S/N ratio, which span from about 4500 to 6800 Å, both in the SARG and FRESCO spectra. To match the lower resolution of FRESCO spectra ($R_{\text{FRESCO}} = 21\,000$) we degraded the resolution of the ELODIE templates by convolving them with a Gaussian kernel of
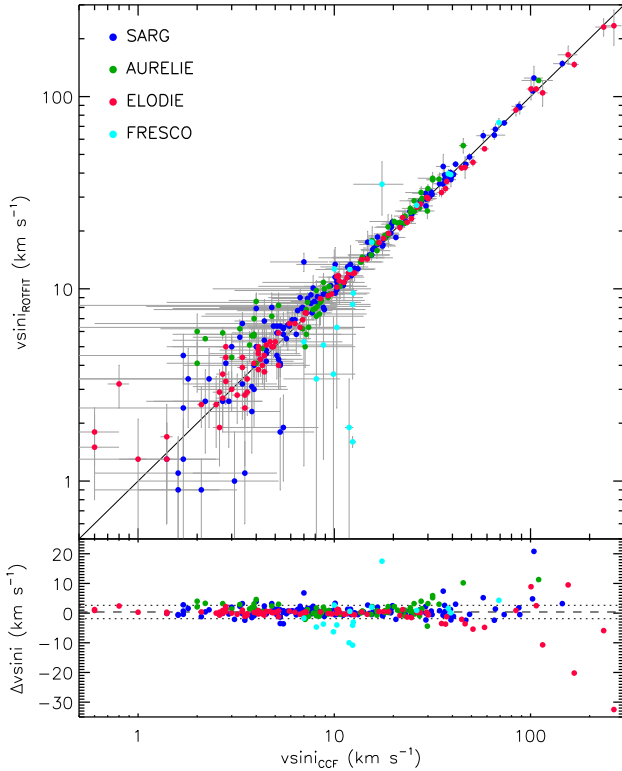
Fig. 1. *Top panel*: comparison between the $v \sin i$ values measured with ROTFIT and those derived from the FWHM of the cross-correlation peak (Table A.1). A different colored dot corresponds to each instrument, as indicated in the legend. The continuous line is the one-to-one relationship. *Bottom panel*: the residuals from the one-to-one relationship, excluding the values with $v \sin i \geq 100\,\mathrm{km\,s^{-1}}$, have a mean of $+0.38\ \mathrm{km\,s^{-1}}$ (dashed line) and a standard deviation of $2.26\ \mathrm{km\,s^{-1}}$ (dotted lines).

width $W = \lambda \sqrt{1/R^2_{\mathrm{FRESCO}} - 1/R^2_{\mathrm{ELODIE}}}$ Å. The same was done for the AURELIE spectra, even though their resolution ($R_{\mathrm{AURELIE}} \simeq 40\,000$) is close to the ELODIE spectra.

All the selected échelle orders were analyzed independently. We excluded from the analysis the cores of Balmer lines, which can be contaminated by chromospheric emission; the Li I $\lambda 6707.8$ line; and the spectral regions severely affected by telluric line absorption or by CCD defects. The final stellar parameters are weighted averages of the results of each ith échelle order, where the weight accounts for both the χ^2_i of the fit (more weight is given to the most closely fitted or higher S/N orders) and the amount of information contained in each spectral order, which is expressed by the total line absorption, $f_i = \int (F_\lambda/F_C - 1)\mathrm{d}\lambda$, where F_λ/F_C is the continuum-normalized spectrum in the ith échelle order. The uncertainties of atmospheric parameters are the standard errors of the weighted means to which we added in quadrature the average uncertainties of the reference stars evaluated as ± 50 K, ± 0.1 dex, and ± 0.1 dex for T_{eff}, $\log g$, and [Fe/H], respectively.

As already explained in Sect. 3.1, ROTFIT also provides us with a measure of the star projected rotational velocity because it iteratively broadens each template spectrum in a wide range of $v \sin i$ and finds the χ^2 minimum. However, the values of $v \sin i$ reported in Table A.1 were obtained using as templates the few inactive and slowly rotating standard stars of Table 2, whose spectra were acquired with the same instrumentation as

for the target spectra. This enabled us to overcome any possible systematic error due to the different resolution.

Finally, the MK classification of the target star is also provided by the code. It is defined by the spectral type and the luminosity class of the reference star that more frequently matches the target spectrum in the different échelle orders.

In Table A.4, we list the stellar parameters, along with their errors ($\sigma_{T_{\mathrm{eff}}}$, $\sigma_{\log g}$, and $\sigma_{\mathrm{[Fe/H]}}$), and the MK classification for the single stars and SB1 binaries. The median errors of the atmospheric parameters are about 100 K, 0.16 dex, and 0.11 dex, for T_{eff}, $\log g$, and [Fe/H], respectively.

For double-lined spectroscopic binaries (SB2) and triple systems we do not determine the atmospheric parameters but we only provide the values of radial and rotational velocities of their components measured thanks to the CCF analysis (cf. Sect. 3.1). The spectral classification and estimates of the atmospheric parameters of the components of SB2s via the COMPO2 code (see, e.g., Frasca et al. 2006) are deferred to a subsequent work devoted to systems with more observations, for which we will also discuss their orbital parameters. However, ten SB2 and one SB3 systems, for which one component is much brighter than the other, have been also analyzed with ROTFIT.

### 3.4. Chromospheric activity and lithium equivalent width

As we did for the optically bright sources (Paper I), we evaluated the level of chromospheric activity from the emission in the core of the Balmer Hα line for the single stars and SB1 systems. A rough age classification was performed based on the lithium abundance (see Sect. 4.3).

We measured both the lithium equivalent width and the chromospheric emission level with the spectral subtraction technique (see, e.g., Herbig 1985; Frasca & Catalano 1994; Montes et al. 1995). This technique is based on the subtraction of a template, which is the spectrum of a slowly rotating star rotationally broadened to the $v \sin i$ of the target. We chose templates with the same spectral type as the target, a negligible level of chromospheric activity, and without any detectable lithium absorption line. This method allows us to remove the Fe I $\lambda 6707.4$ Å absorption line, which is normally blended with the lithium line from the target spectrum. Likewise, the subtraction of the photospheric absorption profile of the non-active template allows us to measure the net chromospheric emission that fills in the Hα line core. Therefore, the equivalent width of the lithium line, W_{Li}, and the net equivalent width of the Hα line, $W^{em}_{\mathrm{H}\alpha}$, were measured in the residual spectrum obtained by subtracting the non-active template. The values of W_{Li} and $W^{em}_{\mathrm{H}\alpha}$ have been obtained by integrating the residual emission (absorption for the lithium line) profile (see Fig. 2). The errors on the equivalent width of Hα and lithium lines, $\sigma_{W^{em}_{\mathrm{H}\alpha}}$ and $\sigma_{W_{\mathrm{Li}}}$, were estimated as the product of the integration range and the mean error per spectral point, which results from the standard deviation of the flux values of the residual spectrum measured at the two sides of the line. The equivalent widths of Hα and lithium lines are reported in Table A.4 together with their errors.

We also evaluated the Hα surface flux (or radiative losses), $F_{\mathrm{H}\alpha}$, and the ratio of the Hα and bolometric luminosity, $R'_{\mathrm{H}\alpha}$[5], which are calculated according to the following equations:

$$F_{\mathrm{H}\alpha} = F_{6563} W^{em}_{\mathrm{H}\alpha}, \tag{1}$$

---

[5] The prime in $R'_{\mathrm{H}\alpha}$ indicates that the photospheric contribution was subtracted as usual in the definition of activity indices.
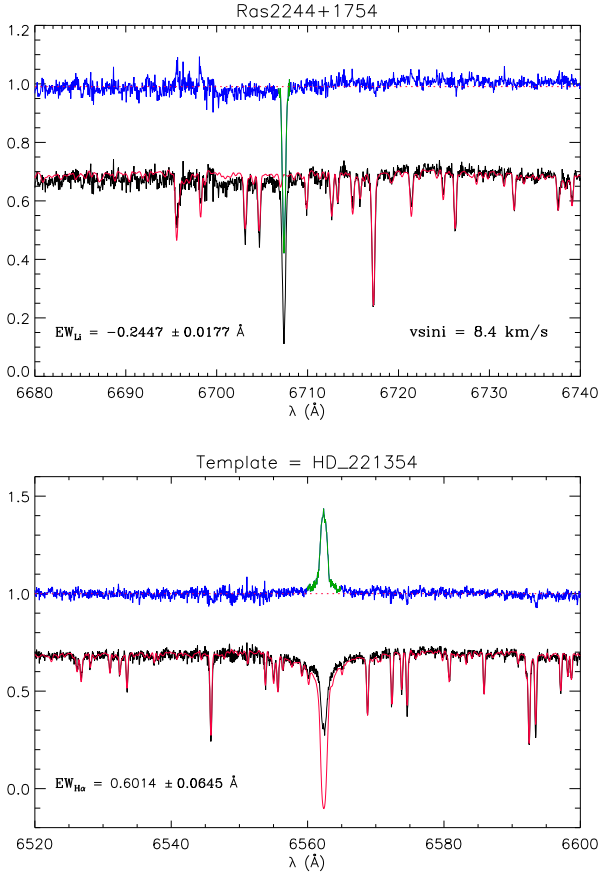
Fig. 2. Example of the subtraction technique applied to an active and lithium-rich star both in the lithium (*upper panel*) and Hα spectral regions (*lower panel*). In *both panels*, the continuum of the residual spectrum (blue line) is set to 1, while the original spectrum (full black line) and the non-active template (thin red line) are shifted downward by 0.3 in continuum units. The green lines indicate the residual absorption (for Li I) or emission (for Hα) profile that has been integrated to obtain the equivalent width.

$$R'_{H\alpha} = L_{H\alpha}/L_{bol} = F_{H\alpha}/(\sigma T_{eff}^4), \qquad (2)$$

where F_{6563} is the continuum flux at the stellar surface at the Hα wavelength, which has been evaluated from the NextGen synthetic low-resolution spectra (Hauschildt et al. 1999) at the stellar temperature and surface gravity of the target. We evaluated the flux error considering the $W_{H\alpha}^{em}$ error and the uncertainty in the continuum flux at the line center, F_{6563}, which is obtained propagating the T_{eff} and $\log g$ errors.

Finally, as far as the lithium line is concerned, we estimated the threshold for lithium line detection as ≈10 mÅ on the basis of typical W_{Li} errors and S/N ratios.

The T_{eff}–$\log g$ diagram of the single and SB1 sources is shown in Fig. 3, where the symbols are color coded according to the value of W_{Li} (Fig. 3a) and $R'_{H\alpha}$ (Fig. 3b).

4. Results

4.1. Binaries and multiple systems

Close binaries are expected to give a large contribution to X-ray selected or chromospherically active stellar samples (see, e.g., Brandner et al. 1996). In fact, the tidal synchronization of the rotation of the components with the orbital period can greatly
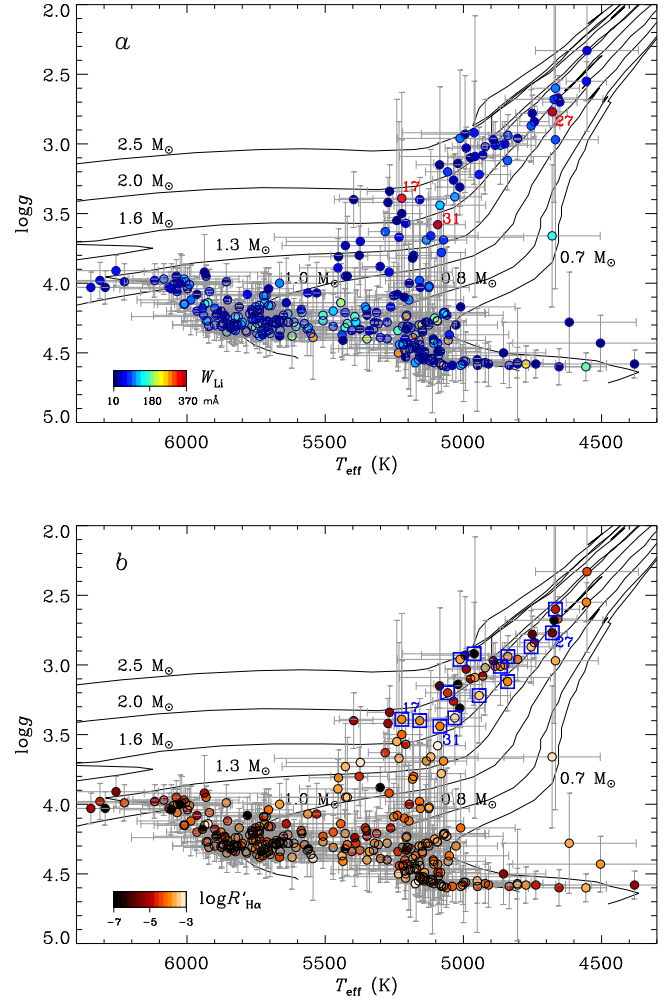
Fig. 3. T_{eff}–$\log g$ diagram for all the single stars and SB1 systems. The symbols are color coded by W_{Li} (*upper panel*) and $R'_{H\alpha}$ (*lower panel*). The black lines are post-MS evolutionary tracks from Girardi et al. (2000) with a metallicity $Z = 0.019$. In the *lower panel*, the lithium-rich giant candidates listed in Table 4 are enclosed in open squares. The two very lithium rich giants (#17 and #27) and the youngest PMS star (#31, see Sect. 4.3) are also indicated.

intensify the magnetic field, and hence the level of activity. Therefore, stellar samples like the *RasTyc* sample allow us to detect close binaries, which can be followed up for the study of their properties. At the same time, they behave as contaminants when looking for young stars. Based on the CCF shape and the variation of the peak centroid, we found 12 SB3 (2.7%), 114 SB2 (25.7%), and 38 SB1 (8.6%) systems. We note that these numbers, especially that of SB1, must be considered as lower limits, since stars with only one observation or even with more spectra could be indeed SB1 systems observed in similar configurations or SB2 close to the conjunctions. Indeed, eight SB1 systems were discovered by the comparison of our single RV value with that reported in the SACY catalog (see Sect. 4.5). Altogether, the close binary systems account for more than 37% of the whole sample. A similar contamination (31%) was estimated for the bright sample in Paper I.

4.2. Hertzsprung-Russell diagram

In Fig. 4, we report the position of the single and SB1 targets with known parallaxes in the HR diagram, which are 263 out
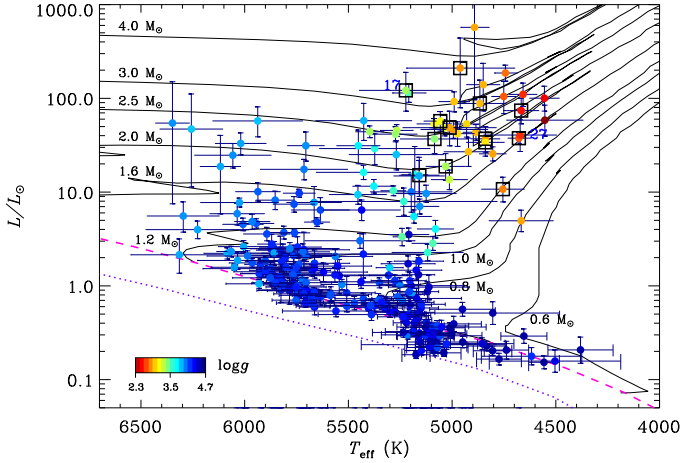
Fig. 4. Hertzsprung-Russell diagram of the single and SB1 sources with known parallaxes. The symbols are color coded by $\log g$. The evolutionary tracks of Girardi et al. (2000) are shown as solid lines with the labels representing their masses. The zero-age main sequence (ZAMS) with solar metallicity ($Z = 0.019$) and with $Z = 0.001$ by the same authors are also shown with a dashed and a dotted line, respectively. The lithium-rich giant candidates listed in Table 4 are enclosed in open squares. The two giants with the highest Li abundance are labeled as in Table 3.

of a total of 328 such targets. We used the $T_{\rm eff}$ values derived with ROTFIT (Table A.4) and the V magnitudes from the *Tycho* catalog that are listed in Table A.1. For most stars (241) the parallaxes are retrieved from the TGAS catalog in the first *Gaia* data release (Gaia Collaboration 2016), while for 22 objects with no entry in that catalog we adopted the values reported by van Leeuwen (2007). The V magnitudes were corrected for the interstellar extinction as in Paper I, i.e., assuming a mean extinction of $A_V = 1.7$ mag/kpc on the Galactic plane ($|b| < 5°$) and 0.7 mag/kpc out of the plane. To convert the V magnitudes to bolometric magnitudes we used the bolometric correction (BC) derived by interpolating the relation $T_{\rm eff}-BC$ of Pecaut & Mamajek (2013). In the same figure we overplot the post-main sequence evolutionary tracks by Girardi et al. (2000).

As apparent in Fig. 4, the values of $\log g$ found from the analysis of the spectra are fully consistent with the evolutionary status of the targets, supporting the reliability of the atmospheric parameters derived by ROTFIT with these spectra.

4.3. Lithium abundance and age

Lithium is burned at relatively low temperatures in stellar interiors ($\sim 2.5 \times 10^6$ K). As a consequence, it is progressively depleted from the stellar atmospheres of late-type stars when mixing mechanisms pull it deeply in their convective layers. Thus, its abundance can be used as an empirical indicator of age for stars cooler than about 6500 K. A simple and effective way to get an age estimate is a diagram showing the equivalent width of lithium as a function of the color index $(B - V)_0$ together with the upper envelopes of young OCs that serve as boundaries to delimit the various age classes (Fig. 5). Although the stars are not very distant from the Sun, their colors are affected by reddening, which was calculated from the magnitude extinction, A_V (see Sect. 4.2) according to standard extinction law $E(B - V) = A_V/3.1$.

We adopted, as in Paper I, the upper envelopes of the following clusters: the Hyades (Soderblom et al. 1990), the Pleiades
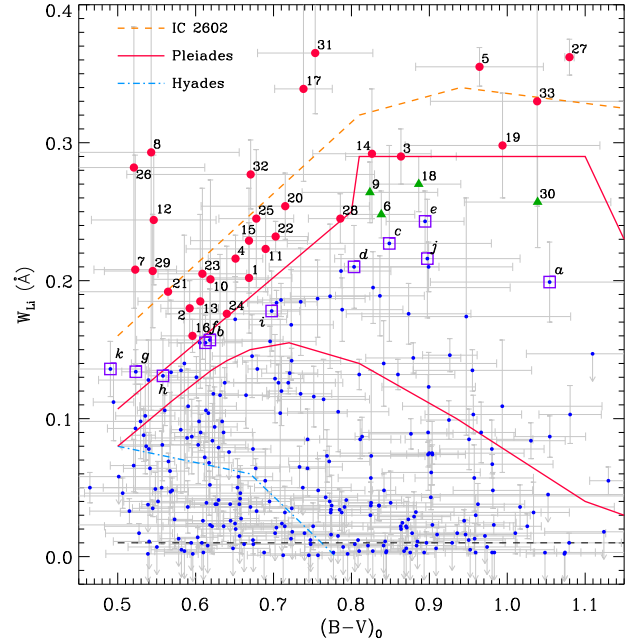
Fig. 5. Equivalent width of the Li I $\lambda 6707.8$ line ($W_{\rm Li}$) plotted as a function of the dereddened Johnson $(B - V)_0$ color index for the single or SB1 stars in our sample (Table A.4). The lines show the upper boundaries for Hyades (blue dash-dotted), Pleiades (red solid for both lower and upper boundary), and IC 2602 (orange dashed) clusters. The black dashed line indicates the lower limit for positive detection of the Li I $\lambda 6707.8$ line estimated by us (10 mÅ). Twenty-nine stars (red big dots) show lithium equivalent width in excess with respect to the most lithium rich Pleiades stars and 10 of the stars fall above the upper envelope of the PMS cluster IC 2602. Four stars (green triangles) have $W_{\rm Li}$ just below the Pleiades upper envelope. The open squares enclose another 11 very young objects selected on the basis of their lithium abundance (see text and Fig. 6). All the lithium-rich stars are labeled according to Table 3.

(Soderblom et al. 1993c; Neuhäuser et al. 1997), and IC 2602 (Montes et al. 2001a), whose ages are of about 650 (White et al. 2007), 125 (White et al. 2007), and 30 Myr (Stauffer et al. 1997), respectively. As shown by Soderblom et al. (1993b), the lower envelope of the Pleiades behaves as an upper boundary for the members of the Ursa Major (UMa) cluster (*age* $\approx$ 300 Myr). Therefore, we considered as pre-main sequence (PMS) or very young star candidates (PMS-like) those stars located above the Pleiades upper envelope (big dots in Fig. 5) or very close to it (triangles) and divided the remaining stars into Pleiades-like, UMa-like, Hyades-like, and Old classes according to their position in the diagram; the Old classes are those with a $W_{\rm Li} < 10$ mÅ. We remark that our selection criterion is not conservative, but it is inclusive; in fact we are not taking into account the errors on $W_{\rm Li}$ and $(B - V)_0$. On the other hand, the upper envelopes of OCs are not knife-like edges that can sharply separate classes of objects of different ages. That is why we used the suffix "like" in our classes. This also means, for example, that the PMS-like class can include stars that are indeed closer to the Pleiades age.

As a further test of our method to select young stars, we calculated the lithium abundance, A(Li), from our values of $T_{\rm eff}$, $\log g$, and $W_{\rm Li}$ by interpolating the curves of growth of Soderblom et al. (1993c). We adopted this calibration to treat our data homogeneously to Sestito & Randich (2005) for the stars in 22 Galactic OCs. In Fig. 6 we show the lithium abundance as a function of $T_{\rm eff}$ along with the upper

**Table 3.** Very young stars and PMS candidates selected from the lithium content.

# Name	$RasTyc$	α (2000) h m s	Δ (2000) ° ′ ″	$C_{rate}^{\sharp}$ (ct/s)	Sp. Type	T_{eff} (K)	$\log g$ (dex)	[Fe/H] (dex)	A(Li)	$\log(R'_{H\alpha})$
#1 BD+78 853[†]	0000+7940	00 00 41.14	+79 40 39.9	0.106	G2V	5738	4.19	−0.03	3.28	−4.43
#2 TYC 4496-780-1[†,‡]	0013+7702	00 13 40.52	+77 02 10.9	0.102	G0V	5924	4.14	−0.03	3.31	−3.33
#3 TYC 4500-1478-1[†]	0038+7903	00 38 06.03	+79 03 20.7	0.133	K1V	5160	4.30	−0.06	3.24	−3.87
#4 BD+78 19[†,★]	0039+7905	00 39 40.13	+79 05 30.8	0.077	G5V	5444	4.14	−0.11	3.05	−4.57
#5 TYC 3266-1767-1	0046+4808	00 46 53.09	+48 08 45.2	0.278	K2V	5067	4.21	−0.09	3.58	−4.02
#6 BD+49 646	0222+5033	02 22 33.82	+50 33 37.8	0.491	K2V	5094	4.27	−0.12	2.84	−3.90
#7 TYC 3695-2260-1	0230+5656	02 30 44.81	+56 56 13.0	0.051	G1V	5874	4.31	−0.03	3.46	−4.47
#8 TYC 2338-35-1	0252+3728	02 52 24.71	+37 28 52.0	0.048	G1.5V	5784	4.35	0.02	4.02	−4.44
#9 TYC 4321-507-1	0300+7225	03 00 14.67	+72 25 41.4	0.084	K2V	5079	4.59	−0.01	2.94	−4.00
#10 Cl Melotte 20 94	0311+4810	03 11 16.82	+48 10 36.9	0.092	G1.5V	5856	4.35	0.02	3.39	−4.24
#11 TYC 3710-406-1	0316+5638	03 16 28.11	+56 38 58.1	0.084	K1V	5208	4.50	−0.05	2.81	−4.18
#12 TYC 3715-195-1	0323+5843	03 23 07.08	+58 43 07.4	0.148	K1V	5212	4.48	−0.07	2.97	−3.92
#13 Cl Melotte 20 935	0331+4859	03 31 28.98	+48 59 28.6	0.081	G1.5V	5816	4.30	−0.10	3.24	−4.05
#14 TYC 2876-1944-1	0359+4404	03 59 16.70	+44 04 17.1	0.264	K1V	5235	4.50	−0.06	3,36	−3.62
#15 TYC 3375-720-1	0616+4516	06 16 46.95	+45 16 03.1	0.097	G2V	5739	4.21	0.11	3.47	−3.83
#16 TYC 3764-338-1	0621+5415	06 21 56.92	+54 15 49.0	0.426	G2V	5719	4.14	−0.08	2.98	−4.15
#17 HD 234808[*]	1908+5018	19 08 14.03	+50 18 49.6	0.045	G8III-IV	5223	3.39	−0.37	3.69	−4.20
#18 KIC 8429280[•]	1925+4429	19 25 01.98	+44 29 50.7	0.254	K2V	5055	4.41	−0.02	2.96	−3.96
#19 BD−03 4778	2004−0239	20 04 49.35	−02 39 19.7	0.175	K1V	5183	4.39	−0.02	3.33	−4.26
#20 HD 332091	2016+3106	20 16 57.83	+31 06 55.6	0.167	K1V	5087	4.57	0.01	2.88	−3.72
#21 TYC 2694-1627-1	2036+3456	20 36 16.87	+34 56 46.1	0.037	G1V	5832	4.33	−0.01	3.30	−4.33
#22 TYC 2178-1225-1	2039+2644	20 39 40.81	+26 44 48.4	0.227	K1V	5149	4.30	−0.08	2.80	−4.19
#23 BD+68 1182	2106+6906	21 06 21.74	+69 06 41.0	0.114	G1.5V	5828	4.31	−0.01	3.39	−4.31
#24 TYC 3589-3858-1	2120+4636	21 20 55.42	+46 36 12.4	0.142	G1.5V	5699	4.36	0.04	3.07	−4.29
#25 BD+76 857a	2223+7741	22 23 18.87	+77 41 57.7	0.114	G1.5V	5745	4.29	−0.04	3.60	−4.28
#26 TYC 1154-1546-1	2233+1040	22 33 00.37	+10 40 34.3	0.053[◇]	G1.5V	5544	4.39	0.03	3.65	−3.44
#27 HD 214995[**]	2241+1430	22 41 57.40	+14 30 59.2	0.094	K0III	4678	2.77	−0.04	3.61	−6.11
#28 BD+17 4799	2244+1754	22 44 41.49	+17 54 19.0	0.835	K1V	5161	4.41	−0.02	2.91	−4.14
#29 TYC 3992-349-1	2246+5749	22 46 13.19	+57 49 58.0	0.034	G2V	5752	4.32	−0.05	3.33	−4.31
#30 TYC 2751-9-1	2307+3150	23 07 24.83	+31 50 14.1	0.462	K4V	4774	4.58	0.05	2.48	−4.15
#31 V395 Cep	2320+7414	23 20 52.07	+74 14 07.1	0.035	K0IV	5093	3.58	−0.02	3.68	−3.27
#32 TYC 584-343-1	2321+0721	23 21 56.36	+07 21 33.0	0.067	K0V	5207	4.24	0.01	3.20	−4.25
#33 TYC 4606-740-1[☉]	2351+7739	23 51 17.29	+77 39 35.3	0.169	K1V	5146	4.52	−0.07	3.51	−3.84
a TYC 2282-1396-1[⊕]	0106+3306	01 06 18.71	+33 06 01.9	0.161	G4V	5606	4.31	−0.14	3.11	−4.16
b BD+42 636	0249+4255	02 49 54.69	+42 55 27.1	0.036	G1.5V	5825	4.24	−0.02	3.07	−4.52
c TYC 3325-98-1	0344+5043	03 44 34.50	+50 43 47.5	0.074	K0V	5349	4.40	−0.06	3.01	−3.99
d TYC 2949-780-1	0646+4147	06 46 46.74	+41 47 12.2	0.043	G2V	5696	4.16	0.13	3.29	−4.60
e TYC 2087-1742-1	1731+2815	17 31 03.33	+28 15 06.1	0.305	K1V	5169	4.47	−0.02	2.91	−3.98
f KIC 7985370[⊗]	1956+4345	19 56 59.73	+43 45 08.2	0.036	G1.5V	5815	4.24	−0.05	3.05	−4.50
g BD+35 4198	2038+3546	20 38 17.71	+35 46 33.3	0.058	G1.5V	5895	4.23	0.01	3.00	−4.86
h BD+39 4490	2114+3941	21 14 55.24	+39 41 11.9	0.099	G1.5V	5930	4.27	−0.02	3.01	−4.75
i TYC 3198-1809-1	2203+3809	22 03 49.83	+38 09 42.9	0.033	G5IV-V	5678	4.28	0.04	3.06	−4.95
j TYC 576-1220-1	2308+0000	23 08 50.46	+00 00 52.8	0.104	G2V	5620	4.38	−0.00	3.25	−3.91
k TYC 4283-219-1	2324+6215	23 24 40.37	+62 15 51.1	0.037	F9V	6011	3.97	−0.21	3.12	−4.84

Notes. [♯] X-ray count rate from the second ROSAT all-sky survey source catalog (2RXS; Boller et al. 2016). [†] PMS star in Cepheus discovered by Guillout et al. (2010). [‡] Close visual pair ($\rho = 1''.41$, $\Delta V \simeq 2.2$ mag; Fabricius et al. 2002). Parameters of the brighter component. [★] SB2 system composed of two nearly identical stars. Parameters derived from spectra taken close to the conjunctions. [•] Very young star in the *Kepler* field discovered by Frasca et al. (2011). [◇] X-ray count rate from the ROSAT All-Sky Bright Source Catalog (1RXS; Voges et al. 1999). [☉] Close visual pair ($\rho = 0''.82$, $\Delta V \simeq 0.15$ mag; Fabricius et al. 2002). [⊕] Close visual pair ($\rho = 0''.85$, $\Delta V \simeq 0.29$ mag; Fabricius et al. 2002). [⊗] Very young star in the *Kepler* field discovered by Fröhlich et al. (2012). [*] Discarded as PMS candidate on the basis of spectral classification and the position in the HR diagram. Likely lithium-rich giant. [**] Discarded as PMS candidate on the basis of spectral classification and the very low Hα flux. Lithium-rich giant.

envelopes of the distributions of some young OCs shown by Sestito & Randich (2005). We note that, contrary to the color indices, the effective temperature does not need to

be corrected for interstellar reddening, and we thereby avoid introducing further uncertainties. Apart from the large errors of A(Li), which take into account both the T_{eff} and W_{Li}
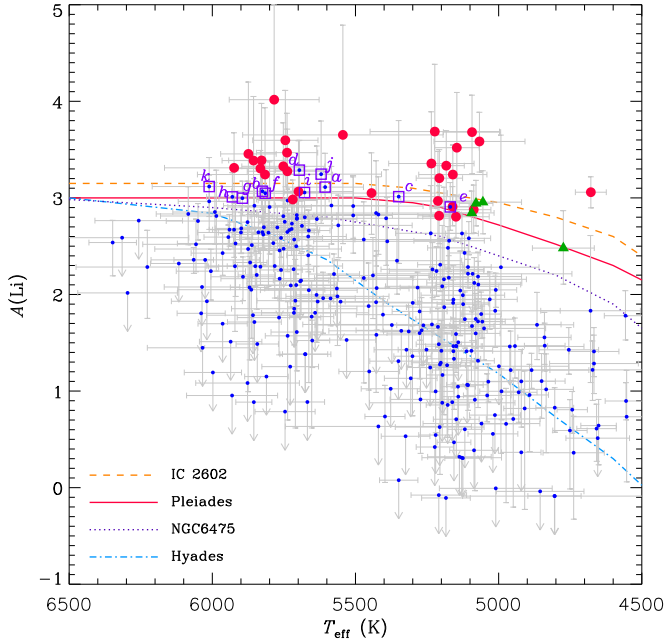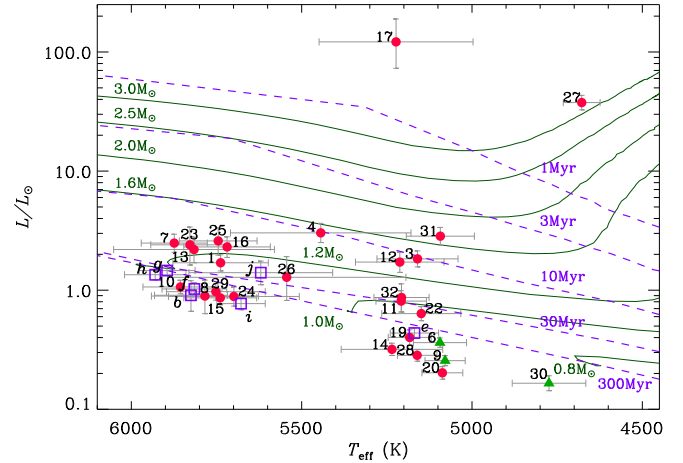
Fig. 6. Lithium abundance as a function of $T_{\rm eff}$ for the stars in Table A.4. The upper envelopes of A(Li) for IC 2602, Pleiades, NGC 6475 (*age* $\approx$ 300 Myr), and Hyades clusters adapted from Sestito & Randich (2005) are overplotted. The meaning of the symbols is the same as in Fig. 5. Another 11 stars with high lithium content are found thanks to this diagram (open squares) and are labeled with letters from *a* to *k*, as in Table 3.

Fig. 7. Hertzsprung-Russell diagram of the PMS-like sources with known parallaxes. The symbols are as in Fig. 5. The PMS evolutionary tracks of Siess et al. (2000) are shown as solid lines with the labels representing their masses. The isochrones at ages of 1, 3, 10, 30, and 300 Myr are shown with dashed lines. The stars labeled as #17 and #27 lie above the 1-Myr isochrone and are likely lithium-rich giants.

errors[6], Fig. 6 clearly shows that all the 33 PMS-like stars already selected from the $W_{\rm Li}$ diagram (Fig. 5), with the exception of only two sources, are located on or above the Pleiades upper envelope. The 2 stars falling just below the Pleiades upper envelope are RasTyc 0316+5638 (#11) and RasTyc 2039+2644 (#22). However, considering the errors, they can be still included in the PMS-like class. Moreover, the 4 stars that lie just below the upper envelope of the Pleiades at $0.8 \leq (B-V)_0 \leq 1.1$ mag in Fig. 1 (green triangles) are located above or exactly superimposed to it in the $T_{\rm eff}$-A(Li) diagram (Fig. 6). In addition, 11 other stars that were not selected on the basis of $W_{\rm Li}$ show a high lithium abundance above the Pleiades A(Li) upper envelope. We indicated these stars with open squares and flagged the stars with letters from *a* to *k* both in Figs. 5 and 6 as well as in Table 3. The inclusion of these targets leads the number of very young star candidates to 44.

In the end, the percentage of PMS-like, Pleiades-like, UMa-like, Hyades-like, and Old stars is about 14%, 13%, 34%, 19%, and 20%, respectively, while for the bright sample (Paper I) they were about 3%, 7%, 39%, 19%, and 32%. Considering the population of very young stars as defined in Paper I, i.e., PMS-like, Pleiades-like, and UMa-like stars taken altogether, their percentage in the faint sample increases from 49% to 61%, while the fraction of the older population decreases of about 10% accordingly. In particular, the fraction of the youngest stars (PMS-like and Pleiades-like) is almost three times higher in the faint sample than in the bright sample.

In an X-ray flux-limited and optically magnitude-limited sample, the fraction of the various populations depends on the X-ray and optical horizons, i.e., the maximum distance at which

we can detect stars in X-ray and at optical wavelengths, respectively. On average, when the X-ray horizon is farther than the optical horizon and the last is increased by changing the limiting magnitude of the sample (fainter stars detected at larger distance), the fraction of young stars increases as well. This can be easily understood because young stars are brighter in X-ray and thus also detectable at larger distances compared to older stars. However, this applies only in general terms because of the role of other stellar parameters in the X-ray luminosity, which depends, inter alia, on both age and mass, making the details more complicated. X-ray population models are absolutely needed for a meaningful interpretation of the observed properties (sky positions, distance distribution, magnitudes, colors, proper motions, etc.) of the *RasTyc* sample. This is out of the scope of the present work and will be the subject of a dedicated paper. We also note that the differences may also arise from the higher incidence of Gould Belt sources in the optically faint sample that reaches beyond the space volume sampled in Paper I.

Figure 7 shows the HR diagram for the PMS-like objects along with the PMS evolutionary tracks and isochrones by Siess et al. (2000). We note that stars #17 and #27 lie above the isochrone at 1 Myr and are likely lithium-rich giants, as also shown in Fig. 4 where they lie close to the post-main sequence tracks for stellar models with 3.0 $M_\odot$ and 1.5 $M_\odot$, respectively. We have therefore disregarded them as PMS-like candidates (see also Table 3 and Appendix B).

4.4. Evolved stars

Besides the two stars mentioned above, a considerable number of giants and subgiants are present among single stars and SB1 systems, as is apparent from the $T_{\rm eff}$–$\log g$ diagram (Fig. 3) and the HR diagram (Fig. 4). Considering as evolved stars those with $\log g \leq 3.5$, we got a sample of 39 out of 328 sources, i.e., 12% of the single+SB1 sources. Half of these also exhibit a remarkable chromospheric emission ($\log R'_{\rm H\alpha} \gtrsim -5$, see Fig. 3b), which is normally paired to a rapid rotation ($v \sin i \gtrsim 9$ km s^{-1}). It is worth noticing that all the SB1 and possible SB2 systems (10 in total) among the 39 evolved stars also display a high chromospheric activity level. The remaining active giants could be

---

[6] We did not consider the errors of $\log g$ for the evaluation of A(Li) errors because an error $\sigma_{\log g} = 0.5$ dex translates into an uncertainty of only a 0.1 or 0.2 dex, at most, in A(Li), in the $T_{\rm eff}$ range of our targets.

Table 4. Lithium-rich giant candidates.

Name	*RasTyc*	Sp. Type	T_{eff} (K)	$\log g$ (dex)	[Fe/H] (dex)	A(Li)	$\log(R'_{H\alpha})$	$v \sin i$ (km s^{-1})
TYC 3676-2444-1	0106+5729	G8III	5158	3.40	−0.05	1.46	−4.22	9.1
TYC 4319-714-1*	0222+7204	K0III-IV	4866	3.01	−0.09	1.69	−4.06	22.3
TYC 4364-1262-1*,†	0712+7021	K1IV	5012	2.96	−0.03	1.83	−3.97	10.3
BD+65 601	0755+6509	K0IV	5085	3.44	−0.07	2.12	−4.35	5.0
TYC 3501-626-1*,◦	1702+4713	K0IV	5031	3.38	−0.05	1.95	−3.55	15.0
BD+06 3372a*	1714+0623	G9III	4839	2.94	−0.10	1.47	−3.96	13.0
BD+02 3384*	1741+0228	G9III	4840	3.12	−0.12	1.56	−4.23	29.3
HD 234808	1908+5018	G8III-IV	5223	3.39	−0.37	3.69	−4.20	8.1
BD−04 5118*	2025−0429	K0III-IV	4943	3.22	−0.05	1.47	−3.63	9.0
BD+48 3149•	2030+4852	K1III	4667	2.60	−0.06	1.41	−5.20	54.1
HD 205173*	2132+3604	K0IV	5057	3.20	0.02	1.72	−5.01	4.1
HD 214995	2241+1430	K0III	4678	2.77	−0.04	3.61	−6.11	5.3
HD 220338*,†,•	2323−0635	K1III-IV	4755	2.87	−0.10	1.43	−3.66	26.8
TYC 3638-993-1	2348+4615	G8III	4961	2.92	−0.03	1.46	…	3.4

Notes. (*) Rotationally variable star (Watson et al. 2015; Kiraga & Stepien 2013). (†) SB1. (◦) Small-amplitude secondary peak in the CCF. Likely SB2 with a faint component. (•) Likely still undergoing the lithium dilution process.

either single stars that are rotating fast as a result of a particular evolutionary path or spectroscopic binaries that are still undetected.

Fourteen out of the 39 evolved stars are lithium-rich giant candidates (A(Li) > 1.4, e.g., Charbonnel & Balachandran 2000). Their properties are summarized in Table 4. Among these stars, only the bright source HD 214995 is already known as a Li-rich giant at the position of the red-giant bump (Charbonnel & Balachandran 2000). The other stars, with the exception of perhaps BD+48 3149 and HD 220338, are hotter than the boundary corresponding to the deepest penetration of the convective zone during the first dredge up (cf. Fig. 1 of Charbonnel & Balachandran 2000), which is around 4400–4600 K for the stars in our mass range. Therefore, these stars have started but not yet completed the standard first dredge-up dilution and should not be considered as abnormally lithium rich. They would exhibit a lithium abundance close to its initial value. As suggested by Fekel & Balachandran (1993), angular momentum may be dredged up from the stellar interior along with Li-rich material during this phase, giving rise to a faster rotation and, consequently, to a higher activity level. This can explain the higher incidence (more than 35%) of lithium-rich giant candidates in our X-ray selected sample compared to the typical fraction of 1 % found in several spectroscopic surveys of giant stars (e.g., de la Reza et al. 2012, and references therein). This is also in line with the high percentage (about 50%) of Li-rich candidates among fast rotating K giants (with $v \sin i \geq 8\,\text{km s}^{-1}$) reported by Drake et al. (2002). It is worth noticing that most of the stars listed in Table 4 are indeed rotating faster than $8\,\text{km s}^{-1}$.

The source TYC 3501-626-1 could be an SB2 system with a faint component on the basis of the CCF. It has a high chromospheric activity level $\log R'_{\text{H}\alpha} = -3.55$ and has been reported as a rotationally variable source ($P_{\text{rot}} \simeq 7.93$ days) by Kiraga & Stepien (2013). The presence of the faint secondary component could have affected the determination of the atmospheric parameters of this star; therefore we cannot exclude that it is a binary system containing young Li-rich stars. In addition, seven of the stars in Table 4, namely TYC 4319-714-1, TYC 4364-1262-1, BD+06 3372a, BD+02 3384, BD-04 5118, HD 205173, and

HD 220338, are also classified as rotationally variable sources by Kiraga & Stepien (2013) and Watson et al. (2015), who have reported photometric periods of 34.5, 35.6, 6.5, 20.4, 39.8, 101.8, and 15.4 days, respectively. With the exception of TYC 4364-1262-1 and HD 220338, which we detected as SB1 systems (see Tables A.1 and A.4), these stars have been observed only once and are therefore preliminarily classified as single stars. We cannot exclude that they are single-lined binaries similar to some long-period RS CVn systems, which also show a fast rotation and lithium enrichment (e.g., Pallavicini et al. 1992; Barrado y Navascués et al. 1998).

4.5. Comparison with the SACY survey

As anticipated in Sect. 2, a similar high-resolution spectroscopic survey of optical counterparts of Southern X-ray sources (SACY) was carried out by Torres et al. (2006). They cross-correlated the RASS catalog with the HIPPARCOS and *Tycho* -2 catalogs to build their sample of stellar X-ray sources and considered only stars with $(B − V) \geq 0.6$, as we have done in Paper I and in the present work. Unlike us, these authors observed stars at all right ascensions, but excluded all HIPPARCOS stars having $M_V < 2.0$ mag to reduce the sample contamination by evolved stars as much as possible. Moreover, they excluded all the already known giants and active binaries of the RS CVn and W UMa classes. This explains the higher incidence of such objects in our survey with respect to SACY.

As we have observed a few stars with a low or negative declination (mainly with SARG), we have some sources in common with the SACY survey. In Table 5 we compare the parameters derived by us for the single stars and SB1 systems with those in the SACY survey. The SACY catalog (Torres et al. 2006) lists the spectral type, RV, W_{Li} for 16 of such sources and $v \sin i$ for 8 of the sources. For 3 other stars da Silva et al. (2009) report W_{Li}, $v \sin i$, and T_{eff} (instead of spectral type), while Elliott et al. (2014) quote their RV values. As shown in Table 5, there is a general good agreement between T_{eff} values (within 150 K), spectral types (within 1–2 spectral subclasses), $v \sin i$ (within 10 %), and W_{Li} (within 10%) with only three exceptions. For

Table 5. Comparison with SACY parameters for single stars and SB1 systems.

RasTyc	Sp. Type/T_{eff} /(K)		$v \sin i$ (km s^{-1})		W_{Li} (mÅ)		RV (km s^{-1})		Notes
	SACY	Present	SACY	Present	SACY	Present	SACY	Present	
0051−1306	G2V	G1V	...	4.5	50	27	3.4	5.10	
0242+3837	4917	5071	6.0	6.4	146	132	−3.46	−3.53	
1959−0432	5630	5752	9.0	9.4	140	126	−19.41	−18.69	
2004−0239	5083	5183	8.0	9.0	290	298	−16.46	−15.92	
2118−0631	K1IV	K1V	...	20.9	40	48	−23.3	22.82	SB1
2155−0947	K0V	G1.5V	...	44.4	0	39	−20.0	−34.35	SB1
2157−0753	K2IV	K1V	...	28.2	0	17	6.7	14.05	SB1
2202−0406	K2V	K1V	...	8.0	200	179	0.3	5.07	SB1
2204+0236	K5V	K5V	...	10.8	0	18	−29.1	−26.36	
2236+0010	K0IV	G8IV-V	...	31.9	0	26	−3.3	7.95	SB1
2256+0235	K1IV	G1.5V	...	33.2	140	106	−9.4	−39.66	SB1
2308+0000	G8V	G2V	39.0	42.8	250	216	7.4	5.30	
2309−0225	K4Ve	K4V	13.3	12.1	200	195	−13.7	−12.16	
2321+0721	K0V	K0V	14.6	14.3	300	277	6.6	6.05	
2323−0635	G9IIIe	K1III-IV	26.4	26.8	105	87	13.4	4.06	SB1
2324−0733	G5V	G5IV-V	4.0	2.5	133	136	4.0	4.00	
2340−0402	G1V	G1V	33.6	36.2	150	128	17.7	15.73	SB1
2340−0228	G2V	G3V	31.0	29.6	0	0	66.3	−20.27	SB1
2352−1143	G1V	G1V	27.8	19.4	115	87	2.6	0.49	SB1

RasTyc 2155−0947 there is a large discrepancy between spectral types. It is an eclipsing binary system according to the ASAS data analyzed by Kiraga (2012). The presence of a secondary component could have affected the spectra giving rise to this large discrepancy. We found a very different spectral type for RasTyc 2256+0235 as well. This source is classified by Kiraga (2012) as a rotationally variable star with a very short period, $P_{rot} = 0.8389$ day. Various T_{eff} determinations are available in the literature, including that of 5316 K (Muñoz Bermejo et al. 2013) based on the same ELODIE spectrum taken by us. This determination is midway between $T_{eff} \simeq 4900$ K corresponding to the SACY K1 IV spectral type (according to the relation of Pecaut & Mamajek 2013) and our value of 5665 K. The distortion of spectral lines and CCF that is likely due to starspots can be responsible for that discrepancy. RasTyc 2352−1143 shows instead a remarkable difference of $v \sin i$ values, which is still larger if compared to the value of 8.2 km s^{-1} reported by Jenkins et al. (2011), who also quote a value of RV= −13.4 ± 1.9 km s^{-1}. This star has been recently discovered to be a close visual binary with a separation of only 0.″22 (Horch et al. 2011).

As regards the RV, we note that 10 objects have very discrepant values and should be considered as SB1 systems. For 8 of these objects, we could collect only one spectrum; therefore, without literature data, we would have preliminarily classified them as single stars.
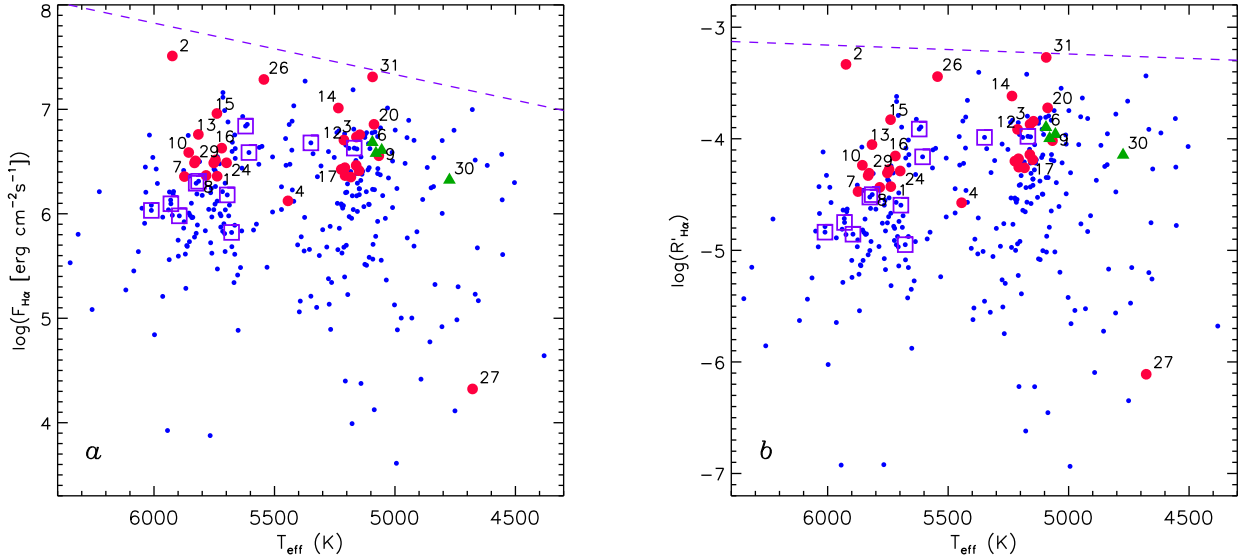
4.6. Chromospheric activity

The Hα fluxes and $R'_{H\alpha}$ indices, plotted against T_{eff}, are shown in Fig. 8, where the boundary between accreting objects and chromospherically active stars, as defined by Frasca et al. (2015), is also shown.

Our targets display a wide range in $R'_{H\alpha}$ with only a few of these sources close to the saturation of magnetic activity, i.e., with $\log(F_{H\alpha}) \geq 6.3$ (e.g., Martínez-Arnáiz et al. 2011, and references therein) or $\log(R'_{H\alpha}) < -4.0$ (e.g., Soderblom et al. 1993a).

There is no object above the activity/accretion boundary, but only the target with the highest Hα flux, namely #31 (V395 Cep), is nearly superimposed to it. This star is classified by Kun et al. (2009) as a classical T Tau star (CTTS) belonging to the L1261 cloud. Indeed, the Hα emission profile displayed by the SARG spectrum is broad and double-peaked, with a central absorption, i.e., it is typical for a CTTS. Moreover, the full width at 10% of the line peak (10%$W_{H\alpha}$) is about 480 km s^{-1}, suggesting an accreting object according to the White & Basri (2003) criterion, 10%$W_{H\alpha} \geq 270$ km s^{-1}. From the Hα luminosity, we have also estimated the mass accretion rate as $\dot{M}_{acc} \simeq 3.6 \times 10^{-9}$ $M_\odot$/yr, following the prescriptions of Biazzo et al. (2012b). This value confirms #31 as a CTTS that displays a significant accretion (e.g., Alcalá et al. 2017). This object is also a class II source, as testified by the large IR excess (see Fig. 9).

The other two stars close to the boundary are #2 (TYC 4496-780-1) and #26 (TYC 1154-1546-1). The former belongs to a small group of young stars discovered by Guillout et al. (2010) in the surroundings of the Cepheus flare region (e.g., Tachihara et al. 2005, and references therein). It is the only object that displays a substantial IR excess among those in Guillout et al. (2010). Furthermore, its Hα profile is similar to that of a CTTS with a double-peaked shape and 10%$W_{H\alpha} \simeq 510$ km s^{-1}. However, this star is a close visual binary (e.g., Fabricius et al. 2002) that deserves a deeper analysis, which is deferred to a subsequent work. The second star (#26) is an ultrafast rotator ($v \sin i \simeq 234$ km s^{-1}) with a broad and shallow Hα profile filled in by emission. This object is likely a zero-age main sequence (ZAMS) star, as also suggested by the HR diagram (Fig. 7) and by the lack of IR excess (see Fig. 9).

One of the candidate lithium-rich giants, namely #27 (HD 214995) shows a very low Hα emission ($\log(R'_{H\alpha}) = -6.11$), while the other (#17 = HD 234808) has $\log(R'_{H\alpha}) = -4.20$, which is similar to the values of other very young stars in our sample. We note that the former star does not display IR excess, while star #17 shows far-infrared excess (see Sect. 4.7).

Fig. 8. Hα flux (*a*) and $R'_{H\alpha}$ (*b*) as a function of T_{eff}. The symbols are as in Fig. 5. The lithium-rich stars that are not too crowded are labeled according to Table 3. The dashed straight line is the boundary between chromospheric activity (below it) and emission due to accretion as derived by Frasca et al. (2015).

4.7. Spectral energy distributions of very young sources

We analyzed the SED of the very young and PMS-like candidates to check the consistency between the photometry and the stellar parameters derived from our spectra. This analysis also allowed us to detect IR excesses and classify the sources in the Lada (1987) scheme.

We constructed the SED of the *RasTyc* sources using the optical and near-infrared (NIR) photometric data available in the literature. In particular, we used *BVR* photometry from the NOMAD catalog (Zacharias et al. 2004), where the magnitudes in the Johnson *B* and *V* bands are obtained by transformations from *Tycho* B_T–V_T system and the *R* magnitude is normally taken from the USNO-B1.0 catalog (Monet et al. 2003). Whenever available (in a few cases), a more precise simultaneous photometry in the optical bands was adopted instead (e.g., Guillout et al. 2010; Frasca et al. 2011; Fröhlich et al. 2012). For all the sources we retrieved *I* magnitudes from the TASS catalog (Droege et al. 2006) and completed the optical/NIR SED with the 2MASS JHK_s photometry (Cutri et al. 2003; Skrutskie et al. 2006). The mid-infrared (MIR) photometry was retrieved from the AllWISE data release (Wright et al. 2010; Cutri et al. 2013) and, for a few sources, from AKARI (Ishihara et al. 2010) and IRAS (e.g., Helou & Walker 1995; Abrahamyan et al. 2015).

We adopted the grid of NextGen low-resolution synthetic spectra, with $\log g$ in the range 3.5–5.0 and solar metallicity by Hauschildt et al. (1999), to fit the optical-NIR portion (from *B* to *J* band) of the SEDs, following Frasca et al. (2009). In the fitting procedure we fixed T_{eff} and $\log g$ of each target to the values found with the code ROTFIT (Table 3) and let the angular stellar diameter and the extinction A_V vary until a minimum χ^2 was reached. For the stars with known distance, this also provides us with a measure of the stellar radius. We always found low values of A_V, ranging from 0.0 to 0.6 mag, in agreement with the estimates made in Sect. 4.2.

We found a relevant MIR excess only for two stars, RasTyc 0013+7702 and RasTyc 2320+7414 (V395 Cep), which behave as class II IR sources. This classification agrees with their

Hα profiles, which are typical of CTTS. In addition, another star in Cepheus, namely RasTyc 0000+7940 (#1) displays a small MIR excess (class III) in line with its weak-line T Tauri star (WTTS) nature.

4.8. Kinematics of the very young sources

The availability of accurate radial velocities and the *Gaia* DR1 TGAS parallaxes and proper motions (Gaia Collaboration 2016) allowed us to calculate the Galactic space-velocity components for most of the sources investigated in the present paper. We used the outline of Johnson & Soderblom (1987) to compute the velocity components, $U_\odot$, $V_\odot$, and $W_\odot$ and their uncertainties, which we report in a heliocentric, left-handed coordinate system, where $U_\odot$ is directed toward the Galactic anticenter.

Space-velocity components are of great importance to assign membership to a known stellar kinematic group (SKG). We show in Fig. 10 the $(U_\odot, V_\odot)$ and $(V_\odot, W_\odot)$ diagrams for the PMS-like stars, along with the average position of the five major young SKGs discussed in Montes et al. (2001b), namely the IC 2391 supercluster (~50 Myr), the Local Association or Pleiades group (~20–150 Myr Asiain et al. 1999; Montes et al. 2001b), the Castor (~300 Myr), and the Hyades supercluster (~600 Myr). Additional SKGs and loose associations, such as TW Hya (3–15 Myr), β Pic (10–24 Myr), Octans (20–40 Myr), AB Dor (50–150 Myr), and Coma Ber (~400 Myr) have been also considered (e.g., Zuckerman et al. 2001, 2004, 2013; Riedel et al. 2017, and references therein). The locus of the young-disk population (YD; age ≤ 2 Gyr) as defined by Eggen (1996, and references therein) is shown as well.

We note that the two lithium-rich giant candidates, #17 and #27, lie outside the YD locus, which confirms the nature of evolved stars.

Most of the PMS-like sources have $U_\odot$, $V_\odot$, and $W_\odot$ compatible with the Pleiades and/or Castor and/or TW Hya SKGs, which are the youngest SKGs considered in this study. However, #12, #16, #24, and #29 are located far outside of the YD locus in the $(U_\odot, V_\odot)$ plane. With the exception of #16, for which we
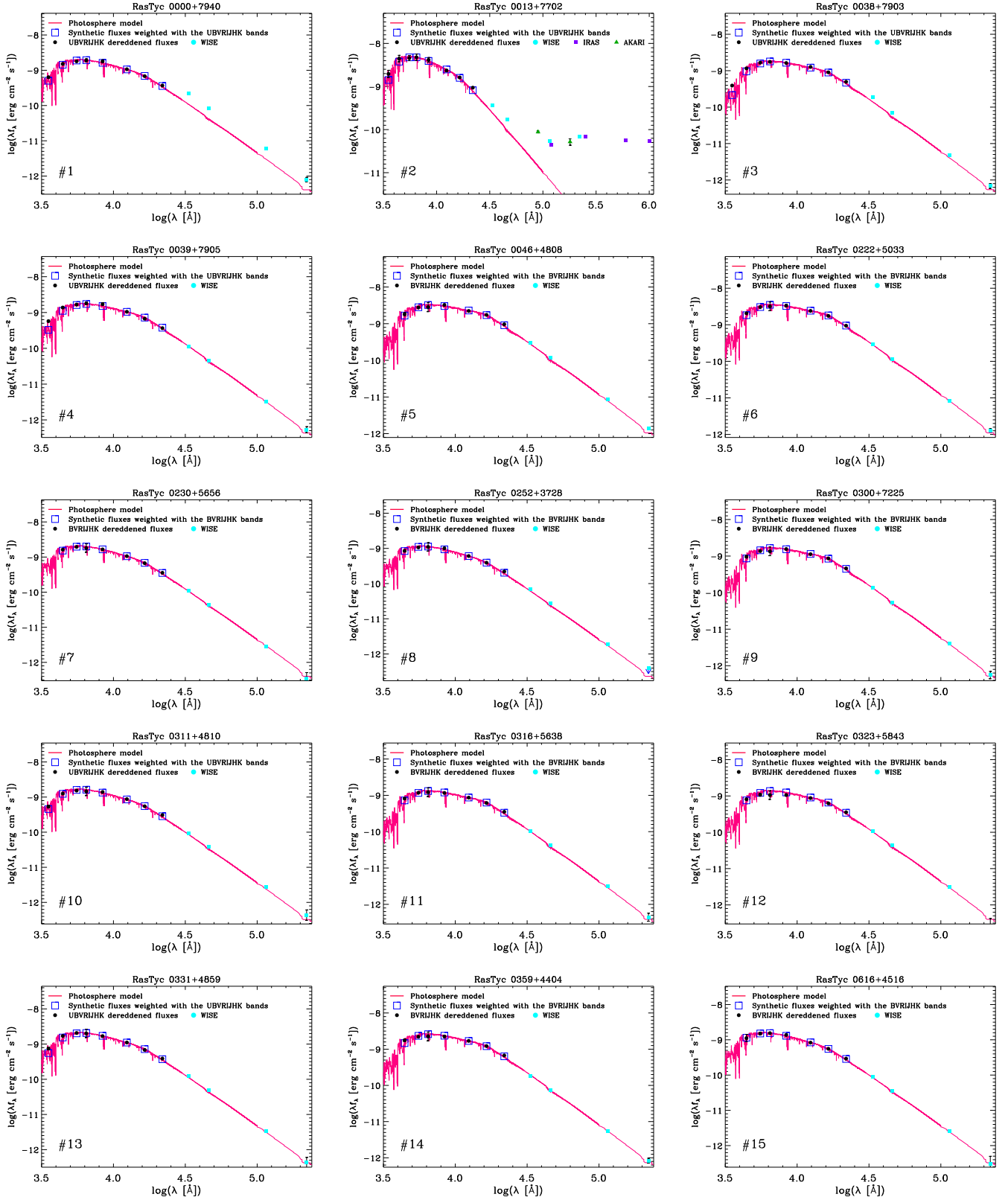
Fig. 9. Spectral energy distributions (dots) of the PMS-like sources and the two lithium-rich giants discussed in the paper. In each panel, the best fitting low-resolution NextGen spectrum (Hauschildt et al. 1999) is shown by a continuous line. Mid-infrared fluxes are shown with different symbols, as indicated in the legends of the plots.

measured the same RV in the two spectra within the errors, the other three sources have been observed only once. Therefore we cannot exclude that they are SB1 systems observed far from the conjunctions, so that their barycentric RV could be very different

from the value measured by us. This would lead to wrong space velocity components.

Some notes about the possible association with the aforementioned SKGs are given in Appendix B.
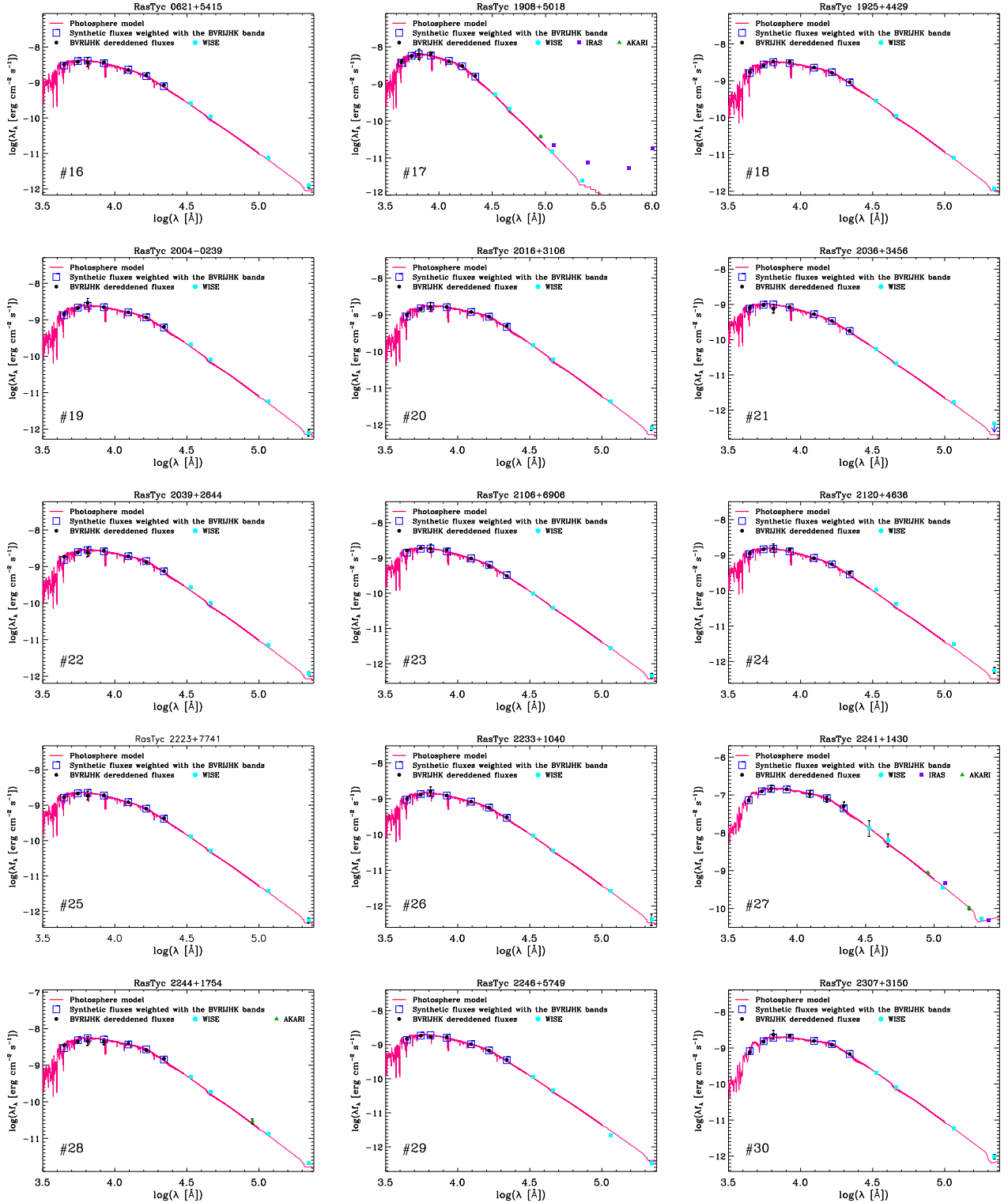
Fig. 9. continued.

5. Summary

We have presented the results of a high-resolution spectroscopic survey of optical counterparts of X-ray sources. Our targets were selected from the *RasTyc* sample (Guillout et al. 1999), which is obtained by the cross-correlation of the *Tycho* and RASS catalogs. In particular, we measured RV and projected rotational velocities ($v \sin i$) for 443 stars, most of which are optically faint *RasTyc* sources ($V \geq 9.5$ mag). We found 114 double-lined

spectroscopic binaries (SB2) and 12 triple systems among these sources.

For the remaining targets, including 38 single-lined binaries (SB1), we were also able to determine the atmospheric parameters (T_{eff}, $\log g$, and [Fe/H]), lithium abundance, and the level of chromospheric activity as measured by the ratio of Hα and bolometric luminosity. The trigonometric parallax from the TGAS catalog (Gaia Collaboration 2016) or from the catalog of van Leeuwen (2007) is also available for 263 of the stars with
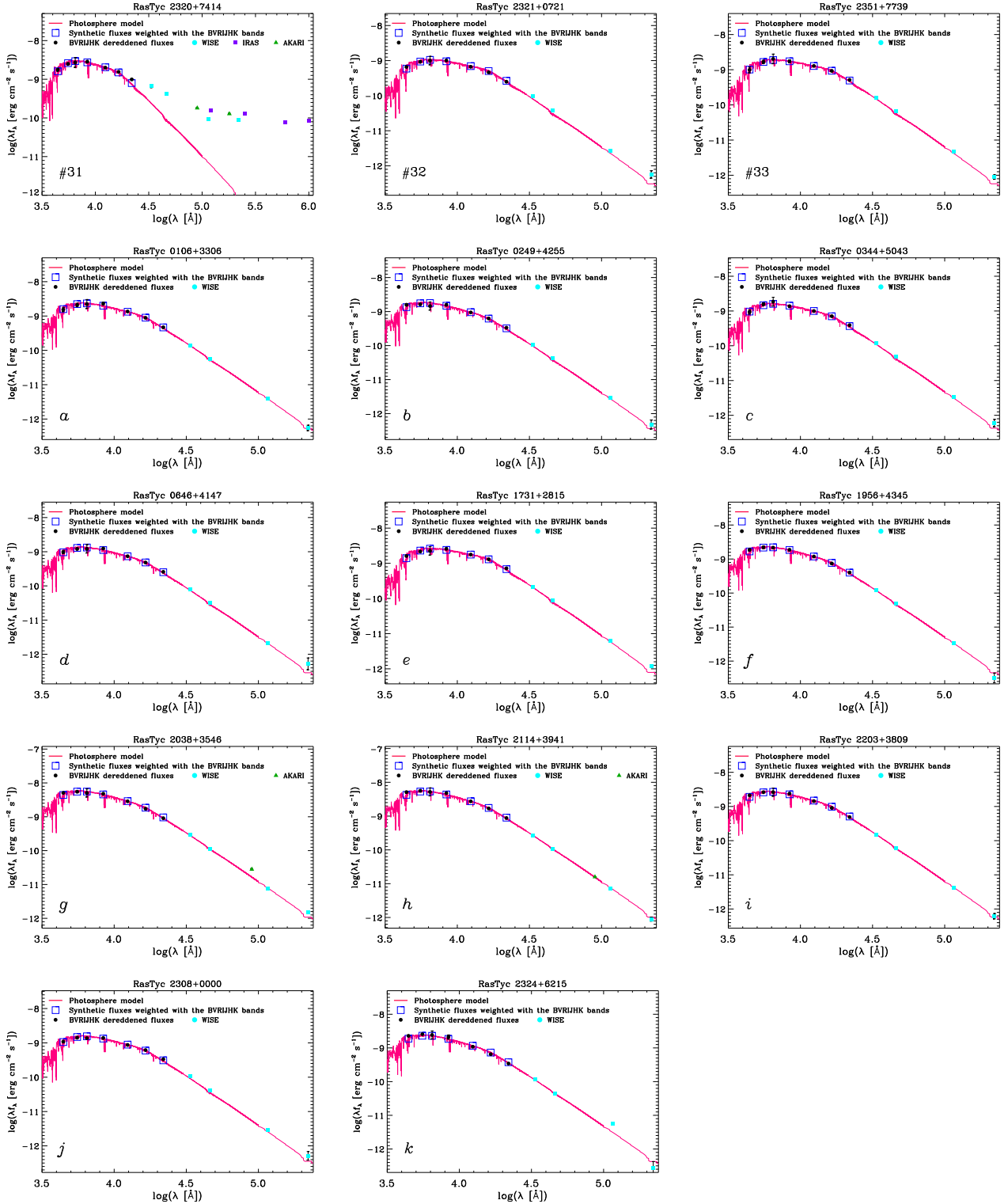
Fig. 9. continued.

measured parameters. The position of these stars in the HR diagram is in very good agreement with the gravities derived with our analysis code (ROTFIT).

The equivalent width of the Li I $\lambda6707.8$ and the lithium abundance allowed us to perform an age classification of our targets that were divided into five classes: PMS-like (14%), Pleiades-like (13%), UMa-like (34%), Hyades-like (19%), and Old stars (20%). The higher percentage of PMS-like and Pleiades-like stars found in comparison with the bright *RasTyc*

sample is likely the result of the greater distances reached in the present work for objects optically fainter. Indeed, at larger distances, the X-ray brighter sources (younger stars) are more easily detected compared to less active (older) stars.

We have investigated in more detail the 44 PMS-like candidates and found that two of these sources must be rejected from this class because their position in the HR diagram, their spectral classification, and their space velocity components
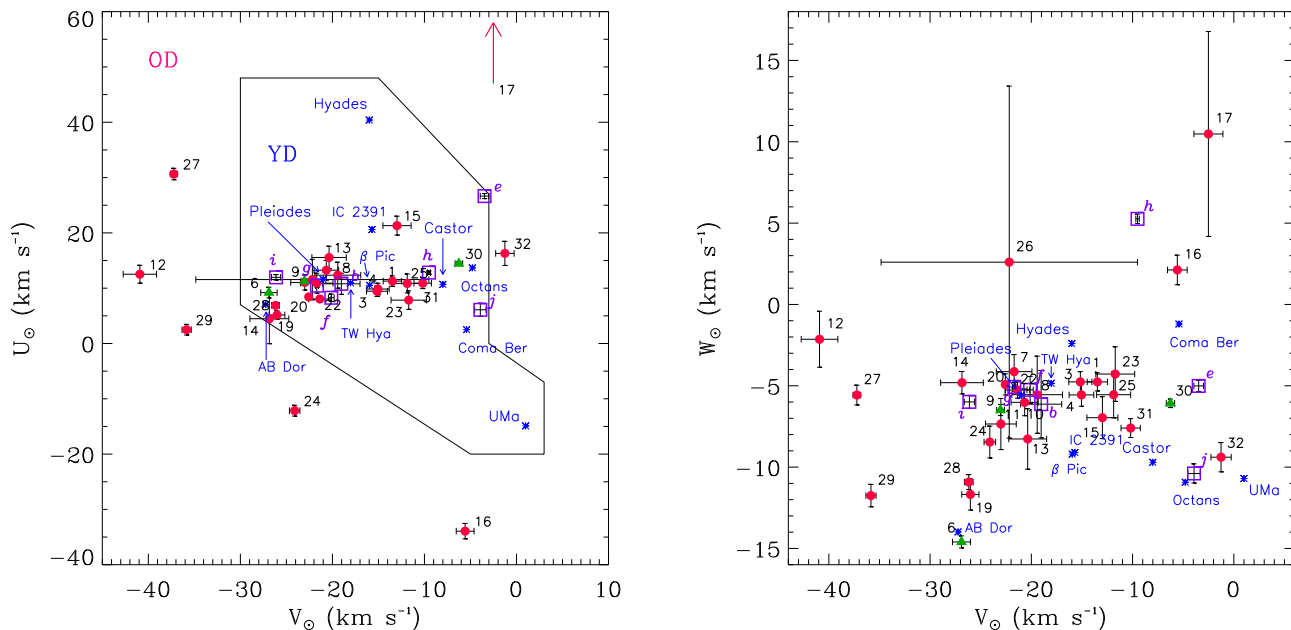
Fig. 10. $(V_\odot, U_\odot)$ (*left panel*) and $(V_\odot, W_\odot)$ (*right panel*) diagrams for PMS-like sources and two lithium-rich giants discussed in the paper. The symbols are as in Fig. 5 and the labels are as in Table 3. The average velocity components (blue asterisks) of some young SKGs and the locus of the YD population (Eggen 1996) are also indicated in the $(V_\odot, U_\odot)$ plane. The position of the source #17 ($V_\odot = -2.5\ \mathrm{km\,s^{-1}}$, $U_\odot = 83.5\ \mathrm{km\,s^{-1}}$) is out of the scale of the plot, as indicated by the red arrow.

suggest they are lithium-rich giants. The remaining PMS-like sources display a rather high level of chromospheric activity, $\log(R'_{H\alpha}) > -5.0$ and, with few exceptions, are located in the domain of the $(V_\odot, U_\odot)$ plane occupied by YD stars. The two objects with the highest values of $R'_{H\alpha}$ (#2 and #31) are very close to the dividing line between chromospheric sources and accreting stars defined by Frasca et al. (2015). They both display a broad and double-peaked Hα profile that is typical of CTTS, as well as a remarkable IR excess in their SEDs.

Another important outcome of this survey is the presence of a significant percentage of giant and subgiant stars ($\sim$12%). Half of these stars also display a high activity level that is comparable to the activity level of some PMS-like sources, and a rather rapid rotation, which could be the result of a particular evolutionary path or the effect of an undetected binarity (spin-orbit synchronization). Some of these evolved stars ($\sim$36%) are also rich in lithium ($A(Li) > 1.4$).

References

Abrahamyan, H. V., Mickaelian, A. M., & Knyazyan, A. V. 2015, Astron. Comput., 10, 99
Alcalá. J. M., Nanara, C. F., Natta, A., et al. 2017, A&A, 600, A20
Ammons, S.M., Robinson, S.E., Strader, J., et al. 2006, ApJ, 638, 1004
Appenzeller, I., Thiering, I., Zickgraf, F.-J., et al. 1998, ApJS, 117, 319
Asiain, R., Figueras, F., & Torra, J. 1999, A&A, 350, 434
Bally, J. 2008, in Handbook of Star Forming Regions, ed. B. Reipurth (ASP Monograph Publications), I, 459
Barrado y Navascués, D., De Castro, E., Fernández-Figueroa, M. J., Cornide, M., & García López, R. J. 1998, A&A, 337, 739
Biazzo, K., Alcalá, J. M., Covino, E., et al. 2012a, A&A, 542, A115
Biazzo, K., Alcalá, J. M., Covino, E., et al. 2012b, A&A, 547, A104
Binks, A. S, Jeffris, R. D., & Maxted, P. F. L. 2015, MNRAS, 452, 173
Bobylev, V. V., 2014, Astrophysics, 57, 583
Boller, T., Freyberg, M. J., Truemper, J., et al. 2016, A&A, 588, A103
Bonchkarev, N. G. 1984, Ap&SS, 138, 229
Brandner, W., Alcalá, J. M., Kunkel, M., Moneti, A., & Zinnecker, H. 1996, A&A, 307, 121
Cameron, A. G. W., & Fowler, W. A. 1971, ApJ, 164, 111
Charbonnel, C., & Balachandran, S. C. 2000, A&A, 359, 563
Christian, D. J., & Mathioudakis, M. 2002, AJ, 123, 2796
Comerón, F., & Torra, J. 1997, A&A, 281, 35
Cutri, R. M., Skrutskie, M. F., Van Dyk, S., et al. 2003, 2MASS All-Sky Catalog of Point Sources, University of Massachusetts and Infrared Processing and Analysis Center (IPAC/California Institute of Technology)
Cutri, R. M., et al. 2013, AllWISE Data Release, IPAC/Caltech University of Massachusetts and Infrared Processing and Analysis Center (IPAC/California Institute of Technology)
da Silva, L., Torres, C. A. O., de La Reza, R., et al. 2009, A&A, 508, 833
de la Reza, R., & Drake, N. A. 2012, ASP Conf. Ser., 464, 51
de la Reza, R., Drake, N. A., & da Silva, L. 1996, ApJ, 456, 115
Desidera, S., Covino, E., Messina, S., et al. 2015, A&A, 573, A126
Dias, W. S., Monteiro, H., Caetano, T. C., et al. 2014, A&A, 564, A79
Dragomir, D., Roy, P., & Rutledge, R. E. 2007, AJ, 133, 2495
Drake, N. A., de la Reza, R., da Silva, L., & Lambert, D. L. 2002, AJ, 123, 2703
Droege, T. F., Richmond, M. W., Sallman, M. P., & Creager, R. P. 2006, PASP, 118, 1666
Eggen, O. J. 1996, AJ, 112, 1595
Elias, F., Alfaro, E. J., & Cabrera-Caño, J. 2009, MNRAS, 397, 2
Elliott P., Bayo, A., Melo, C. H. F., et al. 2014, A&A, 568, A26
Elliott P., Huelamo N., Bouy, H., et al. 2015, A&A, 580, A88
Fabricius, C., Høg, E.; Makarov, V. V., et al. 2002, A&A, 384, 180

Fekel, F. C. 1997, PASP, 109, 514
Fekel, F. C., & Balachandran, S. 1993, ApJ, 403, 708
Feigelson, E. D. 1996, ApJ, 468, 306
Folsom C. P., Petit, P., Bouvier, J., et al. 2016, MNRAS, 457, 580
Frasca, A., & Catalano, S. 1994, A&A, 284, 883
Frasca, A., Freire Ferrero, R., Marilli, E., & Catalano, S. 2000, A&A, 364, 179
Frasca, A., Guillout, P., Marilli, E., et al. 2006, A&A, 454, 301
Frasca, A., Covino, E., Spezzi, L., et al. 2009, A&A, 508, 1313
Frasca, A., Biazzo, K., Kővári, Zs., Marilli, E., & Çakırlı, Ö. 2010, A&A, 518, A48
Frasca, A., Fröhlich, H.-E., Bonanno, A., et al. 2011, A&A, 523, A81
Frasca, A., Biazzo, K., Lanzafame, A. C., et al. 2015, A&A, 575, A4
Fröhlich, H.-E. 2007, Astron. Nachr., 238, 1037
Fröhlich, H.-E., Frasca, A., Catanzaro, G., et al. 2011, A&A, 543, A146
Gaia Collaborations, (Brown, A. G. A., et al.) 2016, A&A, 595, A2
Galicher R., Marois C., Macintosh B., et al. 2016, A&A, 594, A63
Gehrels, N., & Chen, W. 1993, Nature, 361, 706
Gillet, D., Burnage, R., Kohler, D., et al. 1994, A&AS, 108, 181
Girardi, L., Bressan, A., Bertelli, G., & Chiosi, C. 2000, A&AS, 141, 371
Glebocki, R., & Gnacinski, P. 2005, The Catalogue of Rotational Velocities of Stars, ESA SP, 560, 571
Guillout, P., & Motch, C. 2003, Astron. Nachr., 324, 81
Guillout, P., Sterzik, M. F., Schmitt, J. H. M. M., et al. 1998a, A&A, 334, 540
Guillout, P., Sterzik, M. F., Schmitt, J. H. M. M., et al. 1998b, A&A, 337, 113
Guillout, P., Schmitt, J. H. M. M., Egret, D., et al. 1999, A&A, 351, 1003
Guillout, P., Hérent, O., & Motch, C. 2006, in The X-ray Universe 2005, ed. A. Wilson, (ESA SP-604), 89
Guillout, P., Klutsch, A., Frasca, A., et al. 2009, A&A, 504, 829 (Paper I)
Guillout, P., Frasca, A., Klutsch, A., Marilli, E., & Montes, D. 2010, A&A, 520, A94
Gray, D. F. 1992, The Observation and Analysis of Stellar Photospheres, 2nd ed. (Cambridge University Press)
Haakonsen, C. B., & Rutledge, R. E. 2009, ApJS, 184, 138
Hauschildt, P. H., Allard, F., & Baron, E. 1999, ApJ, 512, 377
Helou, G., & Walker, D. W. 1995, Infrared astronomical satellite catalogs and atlases. Vol. 7: The small scale structure catalog – Technical Report (Washington, DC: NASA)
Henden, A. A., Guarro-Flo, J., & Garcia-Melendo, E. 1999, Inf. Bull. Var. Stars, 4807
Henden, A. A., Levine, S., Terrell, D., & Welch, D. L. 2015, APASS - The Latest Data Release, Amer. Astron. Soc. Meet., 225, 336
Herbig, G. H. 1977, ApJ, 214, 747
Herbig, G. H. 1985, ApJ, 289, 269
Herbig, G. H., Bell, K. R. 1988, Lick Observatory Bull. No. 1111
Høg, E., Fabricius, C., Makarov, V.V., et al. 2000, A&A, 355, L27
Hoogerwerf, R. 2000, MNRAS, 313, 43
Horch, E. P., Van Belle, G. T., , Davidson, J. W. Jr., et al. 2015, AJ, 150, 151
Ishihara, D., Onaka, T., Kataza, H., et al. 2010, A&A, 514, A1
Jeffries, R. D. 1995, MNRAS, 273, 559
Jenkins, J. S., Murgas, F., Rojo, P., et al. 2011, A&A, 531, A8
Johnson, D. R. H. & Soderblom, D. R. 1987, AJ, 93, 864
Katz, D., Soubiran, C., Cayrel, R., Adda, M., & Cautain, R. 1998, A&A, 338, 151
Kharchenko, N. V., Piskunov, A. E., Roeser, S., Schilbach, E., & Scholz, R.-D. 2004, Astron. Nachr., 325, 740
Kiraga, M. 2012, Acta Astron., 62, 67
Kiraga, M., & Stepien K. 2013, Acta Astron., 63, 53
Klutsch, A., Frasca, A., Guillout, P., et al. 2008, A&A, 490, 737
Kun, M., Balog, Z., Kenyon, S. J., Mamajek, E. E., & Gutermuth, R. A. 2009, ApJS, 185, 451
Kunder, A., Kordopatis, G., Steinmetz, M., et al. 2017, AJ, 153, 75
Lada, C. J. 1987, in Star forming regions, IAU Symp., 115, 1
Li, J. Z. 2004, Chin. J. Astron. Astrophys., 4, 258
Li, J. Z., Hu, J. Y. 1998. A&AS, 132, 173
López-Santiago, J., Montes, D., Gálvez-Ortiz, M. C., et al. 2010, A&A, 514, A97
Luck, R. E., & Heiter U. 2007, AJ, 133, 2464
Luhman, K. L., Stauffer, J. R., & Mamajek, E. E. 2005, ApJ, 628, L69
Makarov, V. V. 2006, AJ, 131, 2967
Marilli, E., Catalano, S., & Frasca, A. 1997, Mem. Soc. Astron. Ital., 68, 895
Martínez-Arnáiz, R., López-Santiago, J., Crespo-Chacón, I., & Montes, D. 2011, MNRAS, 414, 2629
Mason, B.D., Wycoff, G.L., Hartkopf, W.I., Douglass, G.G., & Worley, C.E. 2001, AJ, 122, 3466

Messina, S., Desidera, S., Turatto, M., Lanzafame, A. C., & Guinan, E. F. 2010, A&A, 520, 15
Metchev, S. A., & Hillenbrand, L. A. 2009, ApJS, 181, 62
Moultaka, J., Ilovaisky, S. A., Prugniel, P., & Soubiran, C. 2004, PASP, 116, 693
Monet, D. G., Levine, S. E., Canzian, B., et al. 2003, AJ, 125, 984
Montes, D., Fernández-Figueroa, M. J., De Castro, E., & Cornide, M. 1995, A&AS, 109, 135
Montes, D., López-Santiago, J., Fernández-Figueroa, M. J., & Gálvez, M. C. 2001a, A&A, 379, 976
Montes, D., López-Santiago, J., Gálvez, M. C., et al. 2001b, MNRAS, 328, 45
Motch, C., Guillout, P., Haberl, F., et al. 1997, A&A 318, 111
Motch, C., Guillout, P., Haberl, F., et al. 1998, A&AS, 132, 341
Muñoz Bermejo, J., Asensio Ramos, A., & Allende Prieto, C. 2013, A&A, 553, A95
Neuhäuser, R., Torres, G., Sterzik, M. F., & Randich, S. 1997, A&A, 325, 647
Nidever, D. L., Marcy, G. W., Butler, R. P., Fischer, D. A. & Vogt, S. S. 2002, ApJS, 141, 503
Nordström, B., Mayor, M., Andersen, J., et al. 2004, A&A, 418, 989
Norton, A. J., Wheatley, P. J., West, R. G., et al. 2008, A&A, 467, 785
Pallavicini, R., Randich, S., & Giampapa, M. S. 1992, A&A, 253, 185
Pecaut, M. J., & Mamajek, E. E. 2013, ApJS, 208, 9
Pigulski, A., Pojman'ski, G., Pilecki, B. & Szczygiel, D. M. 2009, Acta Astron., 59, 33
Piskunov, A. E., Kharchenko, N. V., Schilbach, E., et al. 2008, A&A, 487, 557
Prosser, C. F. 1992, AJ, 103, 488
Queloz, D., Allain, S., Mermilliod, J.-C., Bouvier, J., & Mayor, M. 1998, A&A, 335, 183
Riedel, A. R., Blunt, S. C., Lambrides, E. L., et al. 2017, AJ, 153, 95
Rucinski, S. M., Pribulla, T., Mochnacki, S. W., et al. 2008, AJ, 136, 586
Samus, N. N., Durlevich, O. V., Kazarovets, E. V., et al. 2012, GCVS database, Version 2012 Jan, CDS B/gcvs
Savanov, I. S. 2011, Astron. Rep., 55, 801
Sestito, P. & Randich S. 2005, A&A, 442, 615
Siess, L., Dufour, E., & Forestini, M. 2000, A&A, 358, 593
Soderblom, D. R., Oey, M. S., Johnson, D. R. H., & Stone, R. P. S. 1990, AJ, 99, 595
Soderblom, D. R., Stauffer, J. R., Hudon, J. D., & Jones, B. F. 1993a, ApJS, 85, 315
Soderblom, D. R., Pilachowski, C. A., Fedel, S. B., & Jones, B. F. 1993b, AJ, 105, 2299
Soderblom, D. R., Jones, B. F., Balachandran, S., et al. 1993c, AJ, 106, 1059
Soubiran C., Le Campion J.-F., Cayrel de Strobel G., & Caillo A. 2010, A&A 515, A111
Stauffer, J. R., Hartmann, L. W., Prosser, C. F., et al. 1997, ApJ, 479, 776
Sterzik, M. F., Alcalá, J. M., Neuhaeuser, R., & Schmitt, J. H. M. M. 1995, A&A, 297, 418
Skrutskie, M. F., Cutri, R. M., Stiening, R., et al. 2006, AJ, 131, 1163
Torres, C. A. O., Quast, G. R., da Silva, L., et al. 2006, A&A, 460, 695
Tachihara, K., Neuhäuser, R., Kun, M., & Fukui, Y. 2005, A&A, 437, 919
The HIPPARCOS and Tycho Catalogues, 1997, ESA SP-1200
Udry, S., Mayor, M., & Queloz, D. 1999, Precise Stellar Radial Velocities, IAU Colloq., 170, eds. J. B. Hearnshaw, & C. D. Scarfe, ASP Conf. Ser., 185, 367
Uyama, T., Hashimoto, J., Kuzuhara, M., et al. 2017, AJ, 153, 106
van Leeuwen, F. 2007, A&A, 474, 653
Voges, W., Aschenbach, B., Boller, T., et al. 1999, A&A, 349, 389
Watson, C. L., Henden, A. A., & Price, A. 2015, AAVSO International Variable Star Index VSX - CDS/ADC Collection of Electronic Catalogues
White, R. J., & Basri, G. 2003, ApJ, 582, 1109
White, R. J., Gabor, J. M., & Hillenbrand, L. A. 2007, AJ, 133, 2524
Wright, E. L. Eisenhardt, P. R. M., Mainzer, A.K., et al. 2010, AJ, 140, 1868
Zacharias, N., Monet, D. G., Levine, S. E., et al. 2004, Amer. Astron. Soc. Meeting, 205, #4815, BAAS, 36, 1418
Zickgraf, F.-J., Engels, D., Hagen, H.-J., Reimers, D., & Voges, W. 2003, A&A, 406, 535
Zickgraf, F.-J., Krautter, J. Reffert, S., et al. 2005, A&A, 433, 151
Zinnecker, H. 2008, Workshop on Star Formation Across the Milky Way Galaxy (ESO)
Zuckerman, B., Webb, R. A., Schwartz, M., & Becklin, E. E. 2001, ApJ, 549, L233
Zuckerman, B., Song, I., & Bessell, M. S. 2004, ApJ, 613, L65
Zuckerman, B., Vican, L., Song, I., & Schneider, A. 2013, ApJ, 778, 5

Appendix A: The data

The data resulting from our analysis are listed in Tables A.1–A.4,
which are only available at the CDS.

Table A.1. Radial (RV) and rotational ($v \sin i$) velocities for the single stars and SB1 binaries.

RasTyc Name	Name	α (2000) h m s	Δ (2000) $\circ$ ' ''	V^a (mag)	$B–V^a$ (mag)	HJD (2450000+)	RV (km s^{-1})	σ_{RV}	$v \sin i^b$ (km s^{-1})	$\sigma_{v \sin i}$	$v \sin i^c$ (km s^{-1})	$\sigma_{v \sin i}$	Instr.^{d}
RasTyc0000+7940	BD+78 853	00 00 41.14	+79 40 39.9	10.27	0.704	2224.2896	–6.97	1.10	27.7	4.1	28.9	0.9	AU
RasTyc0000+7940	BD+78 853	00 00 41.14	+79 40 39.8	10.27	0.704	2234.4033	–7.46	2.93	50.3	1.6	...	...	AU
RasTyc0000+7940	BD+78 853	00 00 41.14	+79 40 39.8	10.27	0.704	5109.4942	–7.39	0.52	33.5	0.7	32.1	1.1	FR
RasTyc0000+7940	BD+78 853	00 00 41.14	+79 40 39.8	10.27	0.704	5110.5890	–7.64	0.49	33.5	1.1	32.4	0.9	FR
RasTyc0001+5212	BD+51 3761	00 01 42.66	+52 12 51.0	9.30	0.756	4347.6393	4.97	1.15	5.9	1.7	6.4	0.7	SA
RasTyc0004−0951	HD 225263	00 04 46.96	−09 51 53.4	10.37	0.831	2152.5741	–10.26	0.15	6.9	0.4	6.9	0.7	EL
RasTyc0008+5347	HD 330	00 08 04.62	+53 47 47.0	8.16	0.588	1801.5242	–41.96	0.15	3.2	0.2	2.8	0.8	EL
...	...	...	...	...	...	...	...	...	...	...	...	...	...
...	...	...	...	...	...	...	...	...	...	...	...	...	...

Notes. The full table is available at the CDS.

Table A.2. Radial (RV) and rotational ($v \sin i$) velocities for the components of SB2 binaries.

RasTyc Name	Name	α (2000) h m s	Δ (2000) $\circ$ ' ''	V^a (mag)	HJD (2450000+)	RV_1 (km s^{-1})	σ	RV_2 (km s^{-1})	σ	$v \sin i_1$ (km s^{-1})	σ	$v \sin i_2$ (km s^{-1})	σ	Instr.^{b}
RasTyc0013+7702	TYC 4496-780-1	00 13 40.52	+77 02 10.9	9.76	2226.2918	–1.30	1.57	...	...	31.7	2.3	...	...	AU
RasTyc0013+7702	TYC 4496-780-1	00 13 40.52	+77 02 10.9	9.76	2235.3276	–5.30	1.96	45.27	1.34	41.8	1.4	< 5	...	AU
RasTyc0013+7702	TYC 4496-780-1	00 13 40.52	+77 02 10.9	9.76	5108.5549	–5.78	0.70	44.73	2.74	28.2	9.9	15.6	9.0	FR
RasTyc0013+7702	TYC 4496-780-1	00 13 40.52	+77 02 10.9	9.76	5118.4417	–6.78	0.62	47.27	3.87	30.0	6.7	26.2	7.8	FR
RasTyc0020+5711	TYC 3661-1206-1	00 20 47.59	+57 11 45.1	10.06	2987.2483	–11.78	1.27	–69.15	1.52	22.0	1.4	< 5	...	AU
RasTyc0032+5558	HD 236456	00 32 09.35	+55 58 35.2	9.53	2666.2915	2.75	4.13	–23.93	2.95	< 5	...	55.8	1.2	AU
RasTyc0032+5558	HD 236456	00 32 09.35	+55 58 35.2	9.53	2601.2847	0.85	1.66	–19.42	1.39	< 5	...	43.3	0.5	AU
...	...	...	...	...	...	...	...	...	...	...	...	...	...	...
...	...	...	...	...	...	...	...	...	...	...	...	...	...	...

Notes. The full table is available at the CDS.

Table A.3. Radial (RV) and rotational ($v \sin i$) velocities for the components of SB3 binaries.

RasTyc Name	Name	α (2000) h m s	Δ (2000) $\circ$ ' ''	HJD (2450000+)	RV_1 (km s^{-1})	RV_2 (km s^{-1})	RV_3 (km s^{-1})	$v \sin i_1$ (km s^{-1})	$v \sin i_2$ (km s^{-1})	$v \sin i_3$ (km s^{-1})
				SARG						
RasTyc1831+2515	TYC 2110-348-1	18 31 01.05	+25 15 31.5	4210.7296	–44.89 ± 0.83	71.33 ± 2.10	15.42 ± 0.22	11.2 ± 5.6	17.6 ± 5.8	2.0 ± 2.3
RasTyc2052+4258	BD+42 3895	20 52 57.27	+42 58 25.7	4348.3670	10.18 ± 4.42	–48.46 ± 5.58	–19.20 ± 0.36	9.0 ± 4.3	14.0 ± 12.0	3.4 ± 2.2
RasTyc2259−0431	TYC 5238-1223-1	22 59 02.13	−04 31 35.3	4347.6046	8.68 ± 0.29	–32.54 ± 0.76	–11.60 ± 0.83	2.7 ± 2.0	6.6 ± 2.6	4.2 ± 1.6
...	...	...	...	...	...	...	...	...	...	...
...	...	...	...	...	...	...	...	...	...	...

Notes. The full table is available at the CDS.

Table A.4. Spectral types, atmospheric parameters, and equivalent widths of Li I and Hα lines for the single stars (S) and SB1 binaries.

RasTyc Name	α (2000) h m s	Δ (2000) $\circ$ ' ''	Sp. Type	T_{eff} (K)	$\sigma_{T_{eff}}$	$\log g$ (dex)	$\sigma_{\log g}$	$[Fe/H]$ (dex)	$\sigma_{[Fe/H]}$	W_{Li} (mÅ)	$\sigma_{W_{Li}}$	$W_{H\alpha}^{em}$ (mÅ)	$\sigma_{W_{H\alpha}^{em}}$	Bin^a	Instr.^{b}
RasTyc0000+7940	00 00 41.14	+79 40 39.9	G2V	5738	140	4.19	0.20	–0.03	0.09	202	40	310	50	S	AU+FR
RasTyc0001+5212	00 01 42.66	+52 12 51.0	K1V	5300	103	4.39	0.17	–0.03	0.11	64	20	130	37	S	SA
RasTyc0004−0951	00 04 46.96	−09 51 53.4	K1V	5141	63	4.53	0.14	–0.01	0.11	41	46	5	41	S	EL
RasTyc0008+5347	00 08 04.62	+53 47 47.0	F8V	5944	85	4.18	0.12	–0.12	0.11	69	6	1	6	S	EL
RasTyc0013+7702	00 13 40.52	+77 02 10.9	G0V	5924	243	4.14	0.22	–0.03	0.09	175	10	3900	90	SB2?	AU
RasTyc0013+3946	00 13 58.01	+39 46 02.3	G3V	5707	140	4.31	0.15	–0.07	0.12	40	7	89	9	S	AU
RasTyc0016+4104	00 16 44.88	+41 04 08.6	K3V	5010	197	4.17	0.39	0.03	0.14	2	5	272	38	S	AU
...	...	...	...	...	...	...	...	...	...	...	...	...	...	...	...
...	...	...	...	...	...	...	...	...	...	...	...	...	...	...	...

Notes. The full table is available at the CDS.

Appendix B: Notes on the very young stars and PMS-like candidates

We briefly summarize the known properties of the very young stars and PMS-like candidates listed in Table 3 from the Simbad and Vizier databases and the literature.

#1 RasTyc 0000+7940 (=BD+78 853) was discovered by Guillout et al. (2010) as a WTTS in the surroundings of the Cepheus flare region (e.g., Tachihara et al. 2005, and references therein). Guillout et al. (2010), on the basis of the $v \sin i$ values measured in the two AURELIE spectra, suspected that it was an SB2, but they warned that the different $v \sin i$ may also be the result of a different CCF shape in the two spectral domains. In several spectra subsequently acquired with FRESCO we always measured the same RV, within the errors, and no significant $v \sin i$ variation (see Table A.1). Therefore, we considered this star as a single star. The position on the HR diagram with the Siess et al. (2000) isochrones suggests an age of ≈ 20 Myr (Fig. 7).

#2 RasTyc 0013+7702 (=TYC 4496-780-1) was discovered by Guillout et al. (2010) as a CTTS star, with a broad double-peaked emission, in the surroundings of the Cepheus flare region. They noticed two peaks with a very different height in the CCF that are centered at about 5 and 45 km s^{-1}, which suggests an SB2 system with components of very different luminosity. Other spectra subsequently taken with FRESCO confirm the binary nature of this source (see Table A.2). We assumed that the atmospheric parameters derived with ROTFIT are basically those of the primary component and the effect of the secondary star is negligible because of its faintness. RasTyc 0013+7702 is a also a close visual binary ($\rho = 1\rlap{.}''41$, $\Delta V \simeq 2.2$ mag; Fabricius et al. 2002). The companion was also detected in the H band by the SEEDS survey (Uyama et al. 2017).

#3 RasTyc 0038+7903 (=TYC 4500-1478-1) was discovered as a PMS star by Tachihara et al. (2005), who reported a K1 spectral type. It is one of the four co-moving PMS stars in the Cepheus flare region investigated by Guillout et al. (2010). It is a single star, based on the spectrum appearance and the constant RV. Its position on the HR diagram suggests an age of ≈ 10 Myr (Fig. 7).

#4 RasTyc 0039+7905 (=BD+78 19) was the fourth PMS discovered by Guillout et al. (2010) in the surroundings of the Cepheus flare region. These authors suggested that BD+78 19 may be a binary system of mass ratio ≈ 1. Indeed, our further observations revealed two CCF peaks of the same intensity with a separation of about 25 km s^{-1} in two epochs (see Table A.2). The atmospheric parameters listed in Tables 3 and A.4 were derived from the analysis of the spectra taken at the conjunctions and can be considered as typical for both components. The position on the HR diagram suggests and age of ≈ 10 Myr (Fig. 7). However, considering the system composed of two nearly equal stars, the luminosity of each component should be a factor of two less, bringing these sources closer to the 20 Myr isochrone.

#5 RasTyc 0046+4808 (=TYC 3266-1767-1) is one the stars with the highest W_{Li} in our sample. No specific reference is found in the Simbad database. This object is listed in the catalog of the International Deep Planet Survey (Galicher et al. 2016) as a K3.5-type star with an age between 5 and 30 Myr. The classification is in fairly good agreement with our own (K2). No distance is reported in the *Gaia* DR1 catalog, which prevented us from estimating its age from the position on the HR diagram and studying its kinematical properties.

#6 RasTyc 0222+5033 (=BD+49 646) was proposed as the optical counterpart of the X-ray source RX J0222.5+5033 by Motch et al. (1998) and classified as an active corona source on the basis of the ROSAT hardness ratios. The star is located just below the Pleiades upper envelope in the $(B - V)_0$–W_{Li} diagram (see Fig. 5). The space velocity components are fully compatible with the AB Dor moving group.

#7 RasTyc 0230+5656 (=TYC 3695-2260-1). From its sky location Kharchenko et al. (2004) gave a possible membership to the h and χ Per open clusters. However its magnitude and colors are totally inconsistent with the color–magnitude diagrams of these clusters and the *Gaia* distance of 165 pc, which is much smaller than that of these clusters (~ 2.3 kpc). The position on the HR diagram suggests an age of ≈ 20 Myr (Fig. 7) and its space velocity components are fairly compatible with the Pleiades SKG or the TW Hya association.

#8 RasTyc 0252+3728 (=TYC 2338-35-1) is given as a G5 IV T Tau-type star in Simbad. It is listed in the Washington Visual Double Star (WDS) catalog (Mason et al. 2001) as a close physical visual binary with a separation of $0\rlap{.}''6$ and components of 9.34 and 10.77 mag in the K band; a third component of 13.4 mag separated by $4\rlap{.}''9$ is reported in the same catalog, but it is not given as a physical component. Li & Hu (1998) reported an $W_{\mathrm{H}\alpha}^{em} = 0.50$ Å and $W_{\mathrm{Li}} = 220$ mÅ. Li (2004) classifies the system as a WTTS candidate with proper motions consistent with the Pleiades. From their survey with adaptive optics of young solar analogs Metchev & Hillenbrand (2009) estimated an age of about 200 Myr and a mass $M = 1.1\,M_\odot$ by adopting a distance of 170 pc. From high-resolution spectroscopy White et al. (2007) found an $W_{\mathrm{H}\alpha}^{em} = 2.29$Å and $W_{\mathrm{Li}} = 166$ mÅ. Moreover they reported RV $= 0.78 \pm 2.20$ km s^{-1} and $v \sin i = 29.59 \pm 1.55$ km s^{-1}, in very good agreement with our determinations. We found a larger lithium EW ($W_{\mathrm{Li}} = 293 \pm 187$ mÅ) but with a large error, due to the low S/N of our spectrum. We confirm that the space velocity components are compatible with the Pleiades SKG.

#9 RasTyc 0300+7225 (=TYC 4321-507-1) This star is located just below the Pleiades upper envelope in the $(B - V)_0$–W_{Li} diagram (see Fig. 5). The position in the HR diagram is close to the ZAMS. The space velocity components are compatible with the Pleiades SKG.

#10 RasTyc 0311+4810 (=Cl Melotte 20 94) is given as a rotationally variable F9V star in Simbad. Prosser (1992) classified it as a photometric member of the α Per cluster ($d = 185$ pc, age $= 72$ Myr). From kinematic parameters and a distance of 190 pc assumed for the center of the α Per cluster, Makarov (2006) estimated for this star an RV $= 2.65$ km s^{-1} and a distance $d = 156$ pc, which are in reasonable agreement with our RV and the TGAS distance of 133 ± 5 pc.

#11 RasTyc 0316+5638 (=TYC 3710-406-1) in the catalog of Hoogerwerf (2000), who reported this star as a member of the α Per OB association. The position on the sky along with the strong lithium line, the strongly filled in Hα line, and its kinematics suggest that it is related to the α Per association.

#12 RasTyc 0323+5843 (=TYC 3715-195-1). In the WISE catalog (Wright et al. 2010) a weak probable variability in the W1 ($3.35\,\mu$m) band is reported. The Hα line, in our SARG spectrum, is totally filled in by core emission that reaches

the local continuum. Its position on the HR diagram suggests an age of ≈ 15 Myr (Fig. 7). However, its space velocity components are far from the known young SKGs. It also lies outside of the locus of the YD population (see Fig. 10). With only one spectrum, we cannot exclude that this source is an SB1 system observed far from the conjunction.

#13 RasTyc 0331+4859 (=Cl Melotte 20 935) is a F9.5V star, in the α Per cluster. From high-resolution spectroscopy Prosser (1992) found RV $= -2.7$ km s^{-1} and $v \sin i = 78$ km s^{-1} and defined the star as a member of α Per cluster. In their analysis of rotation in young OCs Marilli et al. (1997) found $V = 10.05$ mag, $B-V = 0.62$ mag, a rotation period $P_{\rm rot} = 0.275$ d and a variation amplitude of 0.05 mag in the V band. From high-dispersion spectra of young nearby stars White et al. (2007) reported an absorption Hα feature with an equivalent width of 3.02 Å, a lithium absorption with $W_{\rm Li} = 110$ mÅ, RV $= -1.8$ km s^{-1}, and $v \sin i = 64.44$ km s^{-1}. On our SARG spectrum we measured nearly the same $v \sin i$ (66.2 km s^{-1}), a slightly higher radial velocity (RV $= 3.35 \pm 2.17$ km s^{-1}), and revealed an Hα strongly filled in by core emission.

#14 RasTyc 0359+4404 (=TYC 2876-1944-1) is given as a rotationally variable star in Simbad. The variability with a period $P_{\rm rot} \simeq 0.456$ d and a variation amplitude in the V band of 0.18 mag has been detected by ASAS (Kiraga & Stepien 2013). We found an RV variation of about 11 km s^{-1} in the two AURELIE spectra, which is, however, just smaller than the sum of the two uncertainties. Therefore, we classified this star as single, but further observations are needed to exclude binarity.

#15 RasTyc 0616+4516 (=TYC 3375-720-1) displays a Hα line that is strongly filled in by core emission in our SARG spectrum. Its kinematics is not far from the average of the IC 2391 supercluster.

#16 RasTyc 0621+5415 (=TYC 3764-338-1) has an age of ≈ 20 Myr based on its position on the HR diagram (Fig. 7). However, its space velocity components are far from the known young associations and moving groups. It is also outside the locus of the YD population (see Fig. 10).

#17 RasTyc 1908+5018 (=HD 234808) was already included in Paper I (the only reference present in the Simbad database), but the data were not analyzed in that paper. The position of this star in the HR diagram is well above the region occupied by the PMS stars and is more consistent with a giant star (see Figs. 4 and 7). The spectral classification (G8III-IV), the $\log g$ value of 3.39 dex and the kinematics strengthen the hypothesis of a lithium-rich giant. This star shows far-infrared excess (see Sect. 4.7 and Fig. 9). The high lithium content of this target could have been synthesized through the Cameron & Fowler (1971) mechanism. This seems to be also supported by the presence of IR excess, which could be due to a dust shell possibly generated via the same mechanism (de la Reza et al. 1996). A conclusive explanation is out of the scope of this work.

#18 RasTyc 1925+4429 (=KIC 8429280) was identified as the optical counterpart of the X-ray source RX J1925.0+4429 by Motch et al. (1998). It is an active star observed by the *Kepler* space telescope whose light curves were analyzed by Savanov (2011) and Frasca et al. (2011) reconstructing the star spot pattern and evolution. In addition to measuring the differential rotation, Frasca et al. (2011) have also measured the atmospheric parameters, RV, $v \sin i$, $W_{\rm Li}$ and chromospheric fluxes from the analysis of SARG

and FRESCO spectra. These data have been also used in the present work. Unfortunately, the *Gaia* DR1 TGAS parallax and proper motions are not available for this source.

#19 RasTyc 2004−0239 (=BD−03 4778) was identified as the optical counterpart of the X-ray source 1RXS J200449.5-023915 by Haakonsen & Rutledge (2009). A lower mass stellar companion ($\Delta K \simeq 2.2$ mag at about $2\farcs5$) was discovered by Elliott et al. (2015).

From high-resolution spectroscopy, da Silva et al. (2009) found $T_{\rm eff} = 5083$ K, $W_{\rm Li} = 290$ mÅ, and $v \sin i = 8$ km s^{-1}. Desidera et al. (2015) reported a K1 V spectral type and values of $T_{\rm eff} = 5160 \pm 30$ K, $v \sin i = 8$ km s^{-1}, and $W_{\rm Li} = 280$ mÅ. Folsom et al. (2016), with high-resolution spectropolarimetry, determined $T_{\rm eff} = 5130 \pm 161$ K, $\log g = 4.45 \pm 0.27$, $v \sin i = 9.6$ km s^{-1}, and measured the magnetic field. These values are close to our determinations ($T_{\rm eff} = 5183 \pm 63$ K, $W_{\rm Li} = 298$ mÅ, $v \sin i = 9$ km s^{-1}). Messina et al. (2010) found it as a member of AB Dor association and measured a rotation period $P_{\rm rot} = 4.68$ d and a full amplitude of the variation in the V band of about 0.10 mag. This star is located just above the Pleiades upper envelope in our $(B - V)_0 - W_{\rm Li}$ diagram (Fig. 5), which indicates an age of ≈ 100 Myr; this is in line with the age adopted by Desidera et al. (2015) and with that of AB Dor (100–125 Myr, Luhman et al. 2005). Its position on the HR diagram is, however, closer to 300 Myr isochrone, but the isochrones at ages larger than 50 Myr are very close to each other for $T_{\rm eff} > 5000$ K, such that they are not very useful to infer ages in this case. The space velocity components derived by us (Fig. 10) confirm the membership to the AB Dor association.

#20 RasTyc 2016+3106 (=HD 332091) was identified as the optical counterpart of the X-ray source 1RXS J200449.5-023915 by Haakonsen & Rutledge (2009). A temperature about 350 K cooler than our value was found by Muñoz Bermejo et al. (2013), who analyzed the same ELODIE spectra acquired by us. We note that our temperature value, $T_{\rm eff} = 5082$ K is closer to the value of 5500 K derived with the Pecaut & Mamajek (2013) calibrations from the dereddened color index $(B - V)_0 = 0.715$ mag than the value $T_{\rm eff} = 4704$ K reported by Muñoz Bermejo et al. (2013). The Hα line is a faint emission feature in all the three ELODIE spectra with a variation of $\approx 30\%$. The kinematics of this star suggest membership to the Pleiades SKG.

#21 RasTyc 2036+3456 (=TYC 2694-1627-1). A temperature about 160 K cooler than our value was found by Muñoz Bermejo et al. (2013) from the analysis of our ELODIE spectrum. The Hα line is filled in by core emission. The kinematics of this star suggest membership to the Pleiades SKG.

#22 RasTyc 2039+2644 (=TYC 2178-1225-1) is given as a rotationally variable star in Simbad. The variability with a period $P_{\rm rot} \simeq 3.485$ d and a variation amplitude in the V band of 0.06 mag has been detected by ASAS (Kiraga & Stepien 2013). The components of the space velocity indicate a possible association with the Pleiades supercluster.

#23 RasTyc 2106+6906 (=BD+68 1182) is a chromospherically active star with the Hα line filled in by core emission and $v \sin i \simeq 40$ km s^{-1}. Both the position on the HR diagram (Fig. 7) and on the $(B - V)_0 - W_{\rm Li}$ diagram (Fig. 5) indicate a PMS object with an age of ≈ 20–30 Myr. Its space-velocity components are close to those of the other stars in the Cepheus flare region discovered by Guillout et al. (2010).

Despite the large apparent distance on the sky, both the kinematics and age suggest that RasTyc 2106+6906 could be related to this stellar group.

#24 RasTyc 2120+4636 (=TYC 3589-3858-1) was identified as the optical counterpart of the X-ray source RX J2120.9+4636 by Motch et al. (1997), who derived a spectral type F9V on the basis of medium-resolution spectra. Our spectral classification (G1.5 V) is in fairly good agreement with the previous work. It is classified as a rotationally variable star in Simbad. The variability with a period $P_{\rm rot} \simeq 0.266$ d and a variation amplitude in the V band of 0.08 mag has been detected by ASAS (Kiraga & Stepien 2013). RasTyc 2120+4636 is a very fast rotating star ($v \sin i \simeq 110$ km s^{-1}) with a filled Hα line. Its space velocity components are far from the known young SKGs. It is also outside the locus of the YD population (see Fig. 10). With only one spectrum, we cannot exclude that this source is an SB1 system observed far from the conjunction.

#25 RasTyc 2223+7741 (=BD+76 857a). Both the position on the HR diagram (Fig. 7) and on the $(B - V)_0$–$W_{\rm Li}$ diagram (Fig. 5) indicate a PMS object with an age of $\approx$20 Myr. Its space-velocity components are close to the Castor SKG and Cepheus flare group.

#26 RasTyc 2233+1040 (=TYC 1154-1546-1) was identified as the optical counterpart of the X-ray source RX J2232.9+1040 by Appenzeller et al. (1998). Zickgraf et al. (2005) gave an uncertain spectral type K2V: $T_{\rm eff} = 4836$ K, $v \sin i = 97$ km s^{-1}, and $W_{\rm Li} = 285$ mÅ, which lead to an abundance A(Li) = 2.76. With these parameters, they classified the source as a ZAMS star with a lithium abundance between the lower and upper envelope of the Pleiades. We find a very similar $W_{\rm Li} = 282$ mÅ, but a very different temperature ($T_{\rm eff} = 5544$ K) and projected rotation velocity ($v \sin i = 234$ km s^{-1}). As a consequence of the higher $T_{\rm eff}$, we determine a much higher lithium abundance, A(Li) = 3.65 and the star lies over the Pleiades upper envelope, both in Figs. 5 and 6. We note that the *Tycho* $B - V = 0.558$, which becomes $(B - V)_0 = 0.521$ considering the reddening, is inconsistent with both the Zickgraf et al. (2005) and our $T_{\rm eff}$ determinations. The color listed in the APASS catalog (Henden et al. 2016), $B - V = 0.723$ or $(B - V)_0 = 0.686$, agrees much better with our $T_{\rm eff}$ determination and that of 5361 K by Ammons et al. (2006). This star, owing to the aforementioned inconsistencies, deserves future investigations.

#27 RasTyc 2241+1430 (=HD 214995) was identified as the optical counterpart of the X-ray source RX J2241.9+1431 by Appenzeller et al. (1998). Zickgraf et al. (2005) reported a K0III spectral type, $T_{\rm eff} = 5152$ K, $W_{\rm Li} = 307$ mÅ, A(Li) = 3.36 and classified this star as evolved lithium-rich. The strong lithium line ($W_{\rm Li} = 389$ mÅ) was confirmed by Luck & Heiter (2007). It was originally included in our list of ELODIE targets, but, based on the literature following our observations and on our results, we discard RasTyc 2241+1430 as PMS candidate and confirm its nature as a lithium-rich giant. The values of $T_{\rm eff}$ and $\log g$ listed in the PASTEL catalog (Soubiran et al. 2010) are in the ranges 4560–4709 K and 2.61–2.70 dex, respectively. Our determinations (Table A.4) are in very good agreement with these values.

#28 RasTyc 2244+1754 (=BD+17 4799) is given as a K2 star in Simbad. This source was selected by Jeffries (1995) as optical counterpart of an extreme ultraviolet source. From intermediate-resolution spectroscopy, he estimated a spectral type K0V/IV, RV spanning from 0.7 to 5.9 km s^{-1}, $W_{\rm Li} \simeq 300$ mÅ, and was also able to obtain a spectrum of a secondary visual component of spectral type M2Ve, $V = 12.7$ mag, and RV $= -2.5$ km s^{-1}, with a separation of about 3″; from kinematical analysis the system turned out to belong to the Local Association. From high-resolution spectroscopy, Fekel (1997) found for the primary visual component RV $= -20.2$ km s^{-1}, suggesting a SB1 behavior, and $v \sin i = 11.4$ km s^{-1}. Christian & Mathioudakis (2002) gave $v \sin i = 8$ km s^{-1} and $W_{\rm Li} = 244$ mÅ (A(Li) = 2.8) in excellent agreement with our values (see Table A.4). López-Santiago et al. (2010) found from high-resolution spectra an average RV $= -16.4$ km s^{-1}, $v \sin I = 11.03$ km s^{-1} and $W_{\rm Li} = 248$ mÅ, confirming the membership to the Local Association. Their values of Hα equivalent width in the subtracted spectrum, $W_{\rm H\alpha}^{em}$, are in the range 0.51–0.76 Å, in good agreement with our values of 0.60–0.72 Å. The spectrum of this source is shown in Fig. 2. The two RV values measured in our spectra are -16.58 and -15.28 whose difference is larger than the sum of errors. For this reason and from the literature data, we consider this star as SB1. The kinematical properties are still consistent with the Local Association, but the velocity components are closer to the AB Dor association (see Fig. 10).

#29 RasTyc 2246+5749 (=TYC 3992-349-1) has only one reference in Simbad. It has been used as a local photometric standard star by Henden et al. (1999), who provide BVR_CI_C photometry, in a study of two eclipsing variables in Cepheus. Its space velocity components are far from the known young associations. It is also outside the locus of the YD population (see Fig. 10). With only one spectrum, we cannot exclude that this source is an SB1 system observed far from the conjunction.

#30 RasTyc 2307+3150 (=TYC 2751-9-1) is given as a K-type variable star in Simbad. In the General Catalogue of Variable Stars (GCVS; Samus et al. 2012) a period $P_{\rm rot} = 7.7129$ d with an amplitude of 0.04 mag is given. The space-velocity components are fairly consistent with Octans association or Castor group.

#31 RasTyc 2320+7414 (=V395 Cep) is given as a variable star of Orion type in Simbad. Herbig (1977) reported a radial velocity of -10 km s^{-1} with a strong Li I line and a spectral type G5-8Ve. In the Catalog of Emission-Line Stars of the Orion Population, Herbig & Bell (1988) reported emission in the Hα line with an equivalent width of about 8 Å and located the star in the L1259 nebulosity. In a study of PMS stars in the Cepheus flare region, Kun et al. (2009) classified this object as a CTTS belonging to the L1261 cloud. With the exception of the two lithium-rich giants, this is the star with the highest position on the HR diagram, close to the 5 Myr isochrone of Siess et al. (2000). Our SARG spectrum displays a broad double-peaked Hα emission profile with a central absorption, which is typical of CTT stars.

#32 RasTyc 2321+0721 (=TYC 584-343-1) is given as a rotationally variable star in Simbad. A rotation period $P_{\rm rot} \simeq 2.5$ d and an amplitude $\Delta V \simeq 0.076$ mag are reported by Watson et al. (2015). Torres et al. (2006) quoted a K0V spectral type, $v \sin i = 14.6$ km s^{-1} and $W_{\rm Li} \simeq 300$ mÅ. Muñoz Bermejo et al. (2013), from the analysis of our ELODIE spectrum, found $T_{\rm eff} = 5221$ K. Our determinations (K0V, $T_{\rm eff} = 5207$ K, $v \sin i = 14.3$ km s^{-1}, $W_{\rm Li} = 277 \pm 25$ mÅ) are in excellent agreement with the aforementioned values from

the literature. A visual companion at $5\farcs1$, which is 2 mag fainter in the J band, has been discovered by Elliott et al. (2015). Both the position on the HR diagram (Fig. 7) and on the $(B - V)_0$–W_{Li} diagram (Fig. 5) indicate a young object with an age of $\approx 30\,\mathrm{Myr}$. Its space-velocity components are just outside the YD locus but they are not far from those of the Octans association.

#33 RasTyc 2351+7739 (=TYC 4606-740-1). In the *Tycho* Double Star Catalogue (Fabricius et al. 2002) it is quoted as a close visual binary with a separation of $0\farcs82$ and components of V magnitudes 11.34 and 11.49 mag. The position on the $(B - V)_0$–W_{Li} diagram (Fig. 5) indicates a PMS-like object on the upper envelope of the IC 2602 cluster (*age* $\approx 30\,\mathrm{Myr}$). Unfortunately, the parallax is not available, preventing us from placing this object on the HR diagram and investigating its kinematical properties.

a RasTyc 0106+3306 (=TYC 2282-1396-1) is quoted as a close visual pair ($\rho = 0\farcs85$, $\Delta V \simeq 0.29\,\mathrm{mag}$; Fabricius et al. 2002). The $B - V$ color reported in *Tycho* catalog ($B - V = 1.092\,\mathrm{mag}$) is probably unreliable as are the individual colors of both components ($B - V \approx 1.0 - 1.1\,\mathrm{mag}$; Fabricius et al. 2002), which are at odds with our spectral classification. This could be due to the binary nature of the source. However, the value of $B - V = 0.646\,\mathrm{mag}$ reported by Henden et al. (2016) agrees much better with our G4V type and $T_{\mathrm{eff}} = 5606\,\mathrm{K}$. With this color RasTyc 0106+3306 would move to the left side in the $(B - V)_0$–W_{Li} diagram (Fig. 5), overcoming the Pleiades upper envelope. The parallax is not available, preventing us from placing this object on the HR diagram and investigating its kinematical properties. Anyway, Dias et al. (2014) considered this star as a member of the cluster Platais 2 (*age* $\sim 350\,\mathrm{Myr}$).

b RasTyc 0249+4255 (=BD+42 636) is given as a G3 star of the NGC 1039 OC ($d = 499\,\mathrm{pc}$, age = 180 My) in Simbad. Kharchenko et al. (2004) found that the star is not a member of NGC 1039. Indeed, the *Gaia* DR1 TGAS distance, $d = 118.3 \pm 13.9\,\mathrm{pc}$, is inconsistent with NGC 1039. The space-velocity components are close to those of the TW Hya association.

c RasTyc 0344+5043 (=TYC 3325-98-1) is reported as a close pair in the WDS catalog (Mason et al. 2001) and has a separation of $0\farcs7$ and components of magnitudes 10.80 and 12.80 mag. This star is well inside the inner radius of the α Per cluster, but its photometry and kinematics exclude membership to the cluster (Kharchenko et al. 2004). The *Gaia* DR1 parallax is not available, preventing us from placing this object on the HR diagram and investigating its kinematical properties.

d RasTyc 0646+4147 (=TYC 2949-780-1) has no specific reference in Simbad.

e RasTyc 1731+2815 (=TYC 2087-1742-1) is quoted as a rotationally variable star in Simbad. The rotation period of about 1.26 d was measured both by SuperWASP (Norton et al. 2007) and ASAS (Kiraga 2012) observations. Dragomir et al. (2007) associated the X-ray source 1RXS J173103.4+281510 with this optical counterpart and classified it as a G/K star from low-resolution spectra. This star was observed spectroscopically by Binks et al. (2015) who found RV = $-18.2 \pm 0.5\,\mathrm{km\,s^{-1}}$, $W_{\mathrm{Li}} = 265 \pm 36\,\mathrm{mÅ}$, and a faint H$\alpha$ absorption line with equivalent width of 0.19 Å. They estimated the age in the range 30–150 Myr, based on W_{Li}, and a lower limit of 37 Myr, on the basis of the Hα and $(V - I)$ color. Our values of RV = $-19.22 \pm 0.62\,\mathrm{km\,s^{-1}}$ and $W_{\mathrm{Li}} = 243 \pm 22\,\mathrm{mÅ}$ are

not significantly different from that of Binks et al. (2015). The Hα line is totally filled in with emission.

f RasTyc 1956+4345 (=KIC 7985370) was discovered as a periodic variable in the field of the *Kepler* space telescope by Pigulski et al. (2009), who found a period $P_{\mathrm{rot}} = 0.4249\,\mathrm{d}$ and amplitudes of 0.04 mag and 0.02 mag in the V and I light curves, respectively. The *Kepler* light curves were analyzed by Fröhlich et al. (2012) who redetermined the period as 2.86 d and reconstructed the starspot distribution and evolution over 229 days with a Bayesian spot model. In addition to measuring the differential rotation, Fröhlich et al. (2012) have also measured the atmospheric parameters, RV, $v \sin i$, W_{Li}, and chromospheric fluxes from the analysis of SARG and FRESCO spectra. These data have also been used in the present work. As already discussed by Fröhlich et al. (2012), the kinematical properties of KIC 7985370 indicate it is a member of the Local Association (Pleiades SKG).

g RasTyc 2038+3546 (=BD+35 4198) was included in the bright catalog (Paper I) but the ELODIE spectrum was not analyzed with ROTFIT. In the present paper, the analysis of the ELODIE and a new SARG spectrum provided us with revised values of atmospheric parameters, W_{Li}, and $W_{\mathrm{H\alpha}}^{em}$. The value of T_{eff} we find (5895 K) is slightly larger than in Paper I and agrees better with the determination of 5954 K by Muñoz Bermejo et al. (2013). Based on its kinematical properties, it could be a member of the Pleiades SKG.

h RasTyc 2114+3941 (=BD+39 4490) was included in the RasTyc bright catalog (Paper I) but the ELODIE spectrum was not analyzed with ROTFIT. In that paper the parameters were derived from two AURELIE spectra, which provided $T_{\mathrm{eff}} = 5731\,\mathrm{K}$, $W_{\mathrm{Li}} = 101\,\mathrm{mÅ}$, and $W_{\mathrm{H\alpha}}^{em} = 64\,\mathrm{mÅ}$. The ELODIE spectrum is higher quality, especially in terms of its wider spectral range, and provides us with a higher value of T_{eff} (5930 K); this agrees better with the value of 5955 K derived by Muñoz Bermejo et al. (2013). The slightly larger $W_{\mathrm{Li}} = 131 \pm 27\,\mathrm{mÅ}$ measured in the ELODIE spectrum leads to a lithium abundance A(Li)=3.01, which brings the star just above the Pleiades upper envelope in Fig. 6. We also find a higher $W_{\mathrm{H\alpha}}^{em} = 149 \pm 34\,\mathrm{mÅ}$, which is likely due to variations of the chromospheric activity. The $U_\odot$ and $V_\odot$ velocity components are close to Castor, but the $W_\odot$ is not.

i RasTyc 2203+3809 (=TYC 3198-1809-1) has no specific reference in Simbad. We did not find any spectroscopic study in the literature. This object lies under the Pleiades upper envelope in the $(B - V)_0$–W_{Li} diagram (Fig. 5), but it is just above it in the diagram T_{eff}–A(Li) (Fig. 6).

j RasTyc 2308+0000 (=TYC 576-1220-1) is quoted as a PMS star in Simbad. It was associated with the X-ray source RX J2308.8+0001 by Zickgraf et al. (2003). Torres et al. (2006) quoted a G8V spectral type, RV = $7.4\,\mathrm{km\,s^{-1}}$, $v \sin i = 39.0 \pm 9.0\,\mathrm{km\,s^{-1}}$ and $W_{\mathrm{Li}} = 250\,\mathrm{mÅ}$. We find an earlier spectral type (G2V) and a slightly lower $W_{\mathrm{Li}} = 216 \pm 43\,\mathrm{mÅ}$. The $v \sin i$ value of $42.8 \pm 5.2\,\mathrm{km\,s^{-1}}$ agrees with that of Torres et al. (2006), but the RV = $5.30 \pm 0.22\,\mathrm{km\,s^{-1}}$ can be indicative of an SB1 system, even though Torres et al. (2006) did not provide the error of their RV measure. However, an RV variation is also indicated by the value of RV = $1.696 \pm 2.642\,\mathrm{km\,s^{-1}}$ reported in the RAVE 5th data release (Kunder et al. 2017). In this catalog, values for the atmospheric parameters of $T_{\mathrm{eff}} = 6000\,\mathrm{K}$, $\log g = 4.00$, and [Fe/H] = -0.25 are also reported. The effective temperature of $T_{\mathrm{eff}} = 5533\,\mathrm{K}$ derived

by Kunder et al. (2017) with the infrared flux method is in better agreement with our determination of $T_{\rm eff} = 5620 \pm 211$ K. This star lies between the 20- and 30-Myr isochrones in the HR diagram (Fig. 7) and close to the UVW position of Octans association.

k RasTyc 2324+6215 (=TYC 4283-219-1) has no specific reference in Simbad, where an F8 spectral type is reported. The *Gaia* DR1 parallax is not available, preventing us from placing this object on the HR diagram and investigating in detail its kinematical properties.